

Submitted to the Astronomical Journal

Abundances in Stars from the Red Giant Branch Tip to the Near the Main Sequence Turn Off in M71: III. Abundance Ratios ¹

Solange V. Ramírez ² and Judith G. Cohen².

ABSTRACT

We present abundance ratios for 22 elements with respect to Fe in a sample of stars with a wide range in luminosity from luminous giants to stars near the turnoff in a globular cluster. Our sample of 25 stars in M71 includes 10 giant stars more luminous than the RHB, 3 horizontal branch stars, 9 giant stars less luminous than the RHB, and 3 stars near the turnoff. The analyzed spectra, obtained with HIRES at the Keck Observatory, are of high dispersion ($R=\lambda/\Delta\lambda=35,000$). We find that the neutron capture, the iron peak and the α -element abundance ratios show no trend with T_{eff} , and low scatter around the mean between the top of the RGB and near the main sequence turnoff. The α -elements Mg, Ca, Si and Ti are overabundant relative to Fe. The anti-correlation between O and Na abundances, observed in other metal poor globular clusters, is detected in our sample and extends to the main sequence. A statistically significant correlation between Al and Na abundances is observed among the M71 stars in our sample, extending to $M_V = +1.8$, fainter than the luminosity of the RGB bump in M5. Lithium is varying, as expected, and Zr may be varying from star to star as well.

M71 appears to have abundance ratios very similar to M5 whose bright giants were studied by Ivans *et al.* (2001), but seems to have a smaller amplitude of star-to-star variations at a given luminosity, as might be expected from its higher metallicity. Both extremely O poor, Na rich stars and extremely O rich, Na poor stars such as are observed in M5 and in M13 are not present in our sample of M71 stars.

The results of our abundance analysis of 25 stars in M71 provide sufficient evidence of abundance variations at unexpectedly low luminosities to rule out the mixing scenario. Either alone or, even more powerfully, combined with other recent studies of C and N abundances in M71 stars, the existence of such abundance variations cannot be reproduced within the context of our current understanding of stellar evolution.

Subject headings: globular clusters: general — globular clusters: individual (M71) — stars: evolution – stars:abundances

¹Based on observations obtained at the W.M. Keck Observatory, which is operated jointly by the California Institute of Technology, the University of California, and the National Aeronautics and Space Administration.

²Palomar Observatory, Mail Stop 105-24, California Institute of Technology.

1. INTRODUCTION

Abundance determinations of stars in Galactic globular clusters can provide valuable information about important astrophysical processes such as stellar evolution, stellar structure, Galactic chemical evolution and the formation of the Milky Way. Surface stellar abundances of C, N, O, and often Na, Mg, and Al are found to be variable among red giants within a globular cluster. The physical process responsible for these star-to-star element variations is still uncertain (see the reviews of Kraft 1994 and Pinsonneault 1997, as well as Cohen *et al.* 2001, Paper I).

In order to study the origin of the star-to-star abundance variations, we have started a program to determine chemical abundances of the nearer galactic globular cluster stars. Cohen *et al.* (2001) presents the sample of stars in M71, the nearest globular cluster reachable from the northern hemisphere, and the atmosphere parameters of the program stars. Our sample includes stars over a large range in luminosity: 19 giant stars, 3 horizontal branch (HB) stars, and 3 stars near the main sequence turnoff, in order to study in a consistent manner red giants, horizontal branch stars, and stars at the main sequence turnoff. Our second paper (Ramírez *et al.* 2001, Paper II) discusses the iron abundance in M71. We found that the $[\text{Fe}/\text{H}]$ abundances from both Fe I ($[\text{Fe}/\text{H}] = -0.71 \pm 0.08$) and Fe II ($[\text{Fe}/\text{H}] = -0.84 \pm 0.12$) lines agree with each other and with earlier determinations (Cohen 1983; Gratton *et al.* 1986; Leep *et al.* 1987; Sneden *et al.* 1994). We also found that the $[\text{Fe}/\text{H}]$ obtained from Fe I and Fe II lines is constant within the rather small uncertainties for this group of stars over the full range in effective temperature (T_{eff}) and luminosity. In this third paper of this series, we present our results for abundances of 22 atomic species in our sample of M71 stars.

2. ATOMIC LINE PARAMETERS

The abundance analysis is done using a current version of the LTE spectral synthesis program MOOG (Sneden 1973). A line list specifying the wavelengths, excitation potentials, gf values, damping constants, and equivalent widths for the observed lines is required. The provenance of the equivalent widths, gf values and damping constants is discussed below.

In addition, a model atmosphere for the T_{eff} and surface gravity ($\log(g)$) appropriate for each star and a value for the microturbulent velocity (ξ) are also required for the abundance analysis. We use the grid of model atmospheres from Kurucz (1993b) with a metallicity of $[\text{Fe}/\text{H}] = -0.5$ dex, based on earlier high dispersion iron abundance analysis of M71 (Cohen 1983; Gratton *et al.* 1986; Leep *et al.* 1987; Sneden *et al.* 1994, Paper II). T_{eff} and $\log(g)$ are derived from the broad-band photometry of the stars as described in Paper I. The photometric T_{eff} has an error of ± 75 K for giants and ± 150 K for dwarfs and $\log(g)$ has an error of ± 0.2 dex. The microturbulent velocity is derived as described in Paper II; ξ has an error of ± 0.2 km s $^{-1}$. Table 1, reproduced from Paper II, lists the stellar parameters of our sample of M71 stars.

2.1. Equivalent Widths

The search for absorption features present in our HIRES data and the measurement of their equivalent width (W_λ) was done automatically with a FORTRAN code, EWDET, developed for this project. Details of this code and its features are described in Paper II. The line list identified and measured by EWDET is then correlated to the list of suitable unblended lines with atomic parameters to specifically identify the different atomic lines. The list of unblended atomic lines was created by inspection of the spectra of M71 stars, as well as the online Solar spectrum taken with the FTS at the National Solar Observatory of Wallace, Hinkle & Livingston (1998) and the set of Solar line identifications of Moore, Minnaert & Houtgast (1966).

In Paper II, we derived the $\lambda D - W_\lambda$ relation of the Fe I lines of “the weak line set” (Fe I lines within two sigma levels of the $\lambda D - W_\lambda$ fit, $W_\lambda < 60$ mÅ, and errors less than a third of the W_λ). We used these $\lambda D - W_\lambda$ relations to determine “the good line set” (lines with errors less than a third of the W_λ and with W_λ computed from the derived $\lambda D - W_\lambda$ relations). The W_λ of the lines presented in this paper are also determined using the fit to the $\lambda D - W_\lambda$ relation of the Fe I lines of “the good line set”, except for the C I, O I and Ca I lines, and for the elements that show hyperfine structure splitting (Sc II, V I, Mn I, Co I, Cu I, and Ba II). The equivalent widths of the C I and O I lines were measured by hand, since thermal motions become important at the low atomic weights of these elements and the $\lambda D - W_\lambda$ relations derived for Fe I lines may no longer be valid. For Ca I lines and the lines of elements that show hyperfine structure splitting, we used the equivalent widths measured automatically by EWDET, but did not force them to fit the Fe I $\lambda D - W_\lambda$ relationship due to the probable different broadening mechanisms. Many of the Ca I lines were strong enough to be on the damping part of the curve of growth. The W_λ used in the abundance analysis are listed in Table ?? (available electronically), which also includes the W_λ for the Fe I and Fe II lines used in Paper II.

2.2. Transition Probabilities

Transition probabilities for the lines used in this analysis were obtained from the NIST Atomic Spectra Database (NIST Standard Reference Database #78, see Weise *et al.* (1969); Martin *et al.* (1988); Fuhr *et al.* (1988); Weise *et al.* (1996)) when possible. Nearly 80% of the lines selected as suitable from the HIRES spectra have transition probabilities from the NIST database. For the remaining lines the gf values come from the inverted solar analysis of Thévenin (1989, 1990), corrected by the factors listed in Table 3 which are needed to place both sets of transition probabilities onto the same scale. The correction factor was computed as the mean difference in $\log(gf)$ between the NIST and solar values for the lines in common, which number is given in column 2 of Table 3. Elements not listed in Table 3 have transition probabilities from the NIST database for all their lines utilized here.

Six elements show hyperfine structure splitting (Sc II, V I, Mn I, Co I, Cu I, and Ba II). The

corresponding hyperfine structure constants were taken from Prochaska *et al.* (2000).

2.3. Damping Constants

Most of the Na I and Ca I lines are strong enough for damping effects to be important. For Na I the interaction constants, C_6 , of the van de Waals broadening were taken from the solar analysis of Baumüller *et al.* (1998). Smith & Raggett (1981) studied collisional broadening of 17 Ca I lines. Comparing their experimental results and the predicted values of C_6 obtained using the Unsöld approximation, we found that the experimental C_6 are about 10 times larger than the Unsöld C_6 . Thus for the Ca I we used the experimental C_6 from Smith & Raggett (1981) when available, otherwise we use 10 times the Unsöld approximation. The empirical values of C_6 for Al I and Mg I from Baumüller & Gehren (1996) and Zhao *et al.* (1998), respectively, are also used. We used 4 times the Unsöld approximation for those Al I lines without empirical damping constants. For the lines of all other ions we set C_6 to be twice the Unsöld approximation as was done in Paper II for the Fe I lines following Holweger *et al.* (1991).

2.4. Solar Abundances

We need to establish the solar abundances corresponding to our adopted set of gf values and damping constants. Solar abundance ratios were computed using our compilation of atomic parameters, the Kurucz model atmosphere for the Sun (Kurucz 1993b) and the list of equivalent widths from Moore *et al.* (1966). The results are listed in Table 4. The O abundance from the permitted lines are corrected by a factor of 0.14 dex (see below). There is a general agreement with the meteoric solar abundance ratios from Anders & Grevesse (1989). The difference between our solar abundances and the meteoric solar abundances from Anders & Grevesse (1989) is listed in column 5 of Table 4. This difference is within the standard deviation of our own measurements, with the exception of [Ca/Fe], which is our most deviant abundance ratio. The difference we found is almost the same as the correction factor applied to the solar gf values, listed in Table 3. We use these solar abundance ratios, derived from our choice of atomic line parameters, to compute the abundance ratios for our sample of M71 stars.

2.5. Non-LTE effects

The non-LTE treatment of the oxygen permitted lines is discussed in §3. The K resonance line is strongly affected by non-LTE effects in the Sun (de la Reza & Muller 1975). Takeda *et al.* (2001) carried out statistical equilibrium calculations of the K I line 7699 Å, the only line used in our analysis, for metal poor stars. We applied a non-LTE correction to our results of K abundance as suggested by Takeda *et al.* (2001). The smallest correction applied was -0.12 dex for the cool

giants stars, and the largest correction was -0.7 dex for the HB stars. Without these corrections, a very strong dependence of K abundance on T_{eff} (equivalent to luminosity) was seen.

The aluminium lines are also affected by non-LTE in metal poor stars (Baumüller & Gehren 1997). Unfortunately, the statistical equilibrium calculations of Baumüller & Gehren (1997) included only dwarf stars. Their non-LTE corrections increased with decreasing metallicity, and were larger for the 3961 Å line than for the 6697 Å doublet used in our analysis. Al and all other elements were treated assuming LTE.

3. ABUNDANCE ANALYSIS

Given the stellar parameters from Paper I, we determined the abundances using the equivalent widths obtained as described above. The abundance analysis is done using a current version of the LTE spectral synthesis program MOOG (Snedden 1973). We employ the grid of stellar atmospheres from Kurucz (1993b) to compute the abundances of C, O, Na, Mg, Al, Si, K, Ca, Sc, Ti, V, Cr, Mn, Co, Ni, Cu, Zn, Y, Zr, Ba, and Eu using the four stellar atmosphere models with the closest T_{eff} and $\log(g)$ to each star’s parameters. The abundances were interpolated using results from the closest stellar model atmospheres to the appropriate T_{eff} and $\log(g)$ for each star.

We also determine the abundance of Li using a synthesis of the spectra in the area of the doublet at 6707Å, which, since it is not well resolved, is considered as only one line in Table 5a. The Li abundance is given as $\log \epsilon(\text{Li}) = \log(N_{\text{Li}}/N_{\text{H}}) + 12.0$, where N is number of atoms. In this case, we used the stellar model atmosphere from Kurucz (1993b) with the closest T_{eff} and $\log(g)$ to each star’s parameters.

The abundance ratios, with the exception of [C/Fe], [O/Fe], [Si/Fe] and [Zn/Fe] are computed using the iron abundance from Fe I lines of Paper II, and our solar abundance ratios from Table 4. The computed abundance ratios are listed in Tables 5a - 5e. For O, we computed the abundance ratio from [O I] lines using [Fe/H] determined from Fe I lines. Given their high excitation potentials, the abundance ratios for the permitted O lines as well as the C I, Si I, and Zn I lines were computed using the [Fe/H] from Fe II lines.

There are 14 stars with equivalent widths measured for both the forbidden and the permitted O lines. The difference of the oxygen abundance ratio from forbidden and permitted lines for those 14 stars is plotted against T_{eff} in Figure 1. A clear trend with T_{eff} is observed, which may come from the different excitation potential of the forbidden and permitted lines or non-LTE effects that affect the permitted lines. We tried applying the non-LTE corrections suggested by Gratton *et al.* (1999) to the permitted lines, but the observed T_{eff} trend becomes even steeper. Since the forbidden lines are usually considered to give more reliable abundances (see Meléndez *et al.* 2001, and references therein), we corrected the abundance ratio from the permitted lines by the amount given by the least squares fit shown in Figure 1. The final [O/Fe] listed in Table 5a is the average for each star of the results from the forbidden and the corrected permitted lines. Note that the

a correction of 0.14 dex, which corresponds to the correction at the temperature of the Sun, was applied to the abundances deduced from the permitted lines of O I in the Sun to compute its [O/Fe] the same way as for our M71 sample of stars.

The abundance ratios (absolute abundance for Li) for each star in our M71 sample are plotted against the photometric T_{eff} in Figures 2 to 23. The error bars shown in Figures 2 to 23 correspond to the standard deviation of results of different atomic lines divided by the square root of the number of lines used for each star. The solid line, shown in Figures 3 to 23, is a linear fit weighted by the errors of the respective abundance ratio versus T_{eff} . The dashed line, shown in Figures 3 to 23, indicates the mean abundance ratio and its respective error plotted as an error bar at 3925 K. The error in the mean abundance ratio corresponds to the standard deviation within our sample of stars divided by the square root of the number of stars for which an abundance was derived for that ion.

We estimate the sensitivity of the abundances with respect to the equivalent widths (synthesis for Li) and the stellar parameters in four cases 4000/1.0/1.4, 4250/1.0/1.4, 5000/2.5/1.0 and 5500/4.0/0.6, where the three numbers correspond to $T_{eff}/\log(g)/\xi$. The case 4000/1.0/1.4 has been computed only for elements with high excitation lines, which are more sensitive at lower temperatures. The stellar parameters in these cases span the relevant range of atmospheric parameters for our M71 sample. We estimated the error in the W_λ to be 10% for all the lines, except the ones with hyperfine structure splitting and the ones of the 8 most faintest stars, which were estimated to be 15%. The error of the synthesis of the Li doublet is estimated to be ± 0.1 dex. The results are listed in Table 6, where the range adopted for each parameter is representative of its uncertainty.

Because of the high excitation of the C I and O I lines studied here, these are the specific ions included in our analysis whose derived abundances are most sensitive to T_{eff} . [Ca/H] also has a sensitive dependence on T_{eff} and ξ , because the Ca I lines are all rather strong and have large damping constants. Most of the elements that show hyperfine structure splitting also present a larger sensitivity with respect to the W_λ error, which was estimated to be higher in those cases.

The mean abundance ratios and their errors are listed in Table 7. The statistical error, σ_{obs} , corresponds to the standard deviation of sample of stars divided by the square root of the number of stars and it is a measure of the scatter of the abundance ratio in the sample of M71 stars. In order to quantify the abundance ratio variations within our sample of M71 stars we have to compare the measure of the scatter with the predicted error from the stellar parameters and the measurement of the W_λ (or synthesis for Li). We estimated the predicted error, σ_{pred} , using the following equation:

$$\begin{aligned} \sigma_{pred}^2 = & \Delta W_\lambda(X)^2/N_{lines}(X) + \Delta W_\lambda(Fe)^2/N_{lines}(Fe) + \\ & [\Delta T_{eff}(X) - \Delta T_{eff}(Fe)]^2 + \\ & [\Delta \log(g)(X) - \Delta \log(g)(Fe)]^2 + \\ & [\Delta \xi(X) - \Delta \xi(Fe)]^2 + \\ & [\Delta [\text{Fe}/\text{H}](X) - \Delta [\text{Fe}/\text{H}](Fe)]^2 \end{aligned}$$

where ΔW_λ , ΔT_{eff} , $\Delta \log(g)$, $\Delta \xi$, and $\Delta [\text{Fe}/\text{H}]$ are listed in columns 2, 3, 4, 5 and 6 of Table 7,

N_{lines} is the number of lines used to compute the abundances, X denotes the element under consideration, and Fe denotes either Fe I or Fe II, whichever was used to compute the abundance ratio. Our σ_{pred} ignores covariance among the error terms, which is discussed in detail by Johnson (2002). She shows that these additional terms are fairly small, and will be even smaller in our case, as we have determined $\log(g)$ using isochrones rather than through ionization equilibria (see Paper I). The general small trends seen in Figures 2 to 23 of $[X/Fe]$ slightly increasing toward cooler T_{eff} may result from ignoring the covariance terms (see Johnson 2002).

The predicted errors for each ion are listed in column 4 of Table 7. The maximum abundance trend over the relevant T_{eff} range for each element, Δ_{max} , is also listed in column 6 of Table 7. This parameter, which is not sensitive to star-to-star scatter abundance variations for stars at a given evolutionary state, is the slope of the linear fit of the abundance ratio vs. T_{eff} times the range in T_{eff} ; its error is the error in the slope time the range in T_{eff} covered by the sample of stars in which the ion of interest was observed. The values of Δ_{max} for essentially all elements observed are gratifyingly small, providing evidence to support many of the assumptions made in the course of this analysis, such as that of non-LTE.

A summary of the abundance ratios for our M71 sample is shown in Figure 24. The results for each element are depicted as a box whose central horizontal line is the mean abundance ratio, while the bottom and the top shows its standard deviation, and the vertical lines coming out of the box mark the position of the most deviant points of the sample. The boxes drawn with dotted lines correspond to elements with abundances computed from results of only one line and hence are more uncertain. The thick line on the left side of the box is the predicted error. As seen in Figure 24, those elements where the predicted error is less than σ_{obs} found in our M71 sample are O, Na, Zr, and the special cases of Li and C, each to be discussed in detail later. These are the elements in which we expect to see star-to-star variations in M71 from our data.

4. DISCUSSION

4.1. Fe-peak elements

The abundance ratios of $[Sc/Fe]$, $[V/Fe]$, $[Cr/Fe]$, $[Mn/Fe]$, $[Co/Fe]$, and $[Ni/Fe]$ follow the behavior of iron as expected, showing no significant trend with T_{eff} , and less scatter around the mean than the predicted error. The mean abundance ratios of Sc ($\langle [Sc/Fe] \rangle = +0.08 \pm 0.15$), V ($\langle [V/Fe] \rangle = +0.21 \pm 0.15$), and Ni ($\langle [Ni/Fe] \rangle = +0.05 \pm 0.06$) are consistent with the earlier results of Sneden *et al.* (1994), who analyzed high resolution spectra of ten giant stars in M71, obtaining $\langle [Sc/Fe] \rangle = +0.10 \pm 0.03$, $\langle [V/Fe] \rangle = +0.19 \pm 0.04$, and $\langle [Ni/Fe] \rangle = +0.07 \pm 0.04$. Our abundance ratios of the iron peak elements are also consistent with the results of Leep *et al.* (1987).

4.2. Neutron capture elements

We have detected lines of the neutron capture elements Zr, Ba and Eu. Cameron (1982) and Käppeler *et al.* (1989) analyzed the solar system meteoritic abundances of neutron capture elements to yield accurate breakdowns into *r*- and *s*-process parts for each isotope, which have been summed into fractions for each element by Burris *et al.* (2000). At $[\text{Fe}/\text{H}] < -2.0$, as reviewed by Sneden *et al.* (2001), Zr and Ba are neutron capture element synthesized through *s*-process reactions that occur mainly in low mass asymptotic giant branch (AGB) stars, while Eu is exclusively an *r*-process element.

The abundance ratios of the neutron capture elements, Zr, Ba, and Eu, show no significant trend with T_{eff} , and less scatter around the mean than the predicted error, except for $[\text{Zr}/\text{Fe}]$. In Figure 25, we show the spectra for two stars of similar T_{eff} and different $[\text{Zr}/\text{Fe}]$, 1–56 (4525 K, $[\text{Zr}/\text{Fe}]=-0.44$) and 1–81 (4550 K, $[\text{Zr}/\text{Fe}]=+0.12$) in the region of the Zr line at 6143 Å, which is the strongest Zr I line included in our study. In the spectral range illustrated, there are also two Fe I lines, one Ba II line and one Si I line, whose strengths are similar in both stars. It is possible but not certain that the difference in strength of the Zr line is due to star-to-star abundance variations. Leep *et al.* (1987) analyzed four Zr lines in five bright giant M71 stars to obtain $[\text{Zr}/\text{Fe}] \sim 0.0$ dex.

The abundance of Ba and of Eu are overabundant relative to Fe, as is seen in other clusters (see below). The mean $[\text{Ba}/\text{Eu}]$ ratio of +0.09 is consistent with values observed in halo stars of similar $[\text{Fe}/\text{H}]$ (Burris *et al.* 2000; Gratton & Sneden 1994).

4.3. α -elements

We find that the α -elements Mg, Ca, Si and Ti are overabundant relative to Fe. Our mean $\langle[\text{Ti}/\text{Fe}]\rangle = +0.27 \pm 0.08$ and $\langle[\text{Si}/\text{Fe}]\rangle = +0.21 \pm 0.09$ are very similar to the results of Sneden *et al.* (1994) for ten M71 giant stars ($\langle[\text{Ti}/\text{Fe}]\rangle = +0.48 \pm 0.04$, $\langle[\text{Si}/\text{Fe}]\rangle = +0.31 \pm 0.04$), and also similar to the abundance ratios provided by Leep *et al.* (1987). Our $\langle[\text{Ca}/\text{Fe}]\rangle = +0.42 \pm 0.05$ is higher than the value of Sneden *et al.* (1994) ($\langle[\text{Ca}/\text{Fe}]\rangle = +0.13 \pm 0.03$), but similar to the abundance ratio of +0.58 found by Leep *et al.* (1987). The α -element abundance ratios show no significant trend with T_{eff} , and low scatter around the mean.

$[\text{Mg}/\text{Fe}]$ is known to vary among bright giant stars in some metal poor globular clusters. In NGC 6752 (Gratton *et al.* 2001), M13 (Kraft *et al.* 1993; Shetrone 1996) and M15 (Sneden *et al.* 1997), $[\text{Mg}/\text{Fe}]$ shows a star-to-star range in abundance of about 1.5, 1.2, and 1.0 dex respectively. Our comparison between the observed scatter and the predicted error of $[\text{Mg}/\text{Fe}]$ given in Table 7 indicates no sign of star-to-star variation of magnesium in M71.

4.4. Sodium and Oxygen

The oxygen abundance ratios in our sample of stars in M71 behave differently than the abundance ratios of other elements included in this paper. The scatter in $[\text{O}/\text{Fe}]$ versus T_{eff} shown in Figure 4 strongly suggests that O shows star-to-star variations within the M71 sample. Furthermore, the observed scatter for $[\text{O}/\text{Fe}]$ given in Table 7 is larger than the respective predicted error which include the effects of uncertainties in the determination of the the stellar parameters and in the equivalent width measurements. To a lesser extent, the Na abundances behave similarly, as shown in Figure 5, but the observed scatter for Na is only slightly larger than the value σ_{pred} given in Table 7.

In Figure 26 we compare the strength of the Na I and O I lines between two stars of similar stellar parameters. The star with the highest $[\text{O}/\text{Fe}]$ in our sample (1–60) has a low $[\text{Na}/\text{Fe}]$ and the star with lowest $[\text{O}/\text{Fe}]$ (2–160) has an intermediate $[\text{Na}/\text{Fe}]$. These two stars are marked with open squares in Figures 4 and 5, and represent the extremes of the set of O abundances for the M71 sample. Note that both of these stars are red giants fainter than the HB, with $M_V = +1.4$ for the fainter, Na-richer star. This figure demonstrates that the higher scatter seen in $[\text{Na}/\text{Fe}]$ and $[\text{O}/\text{Fe}]$ is due to star-to-star abundance variations and that in the case of this specific pair of stars, Na and O are anti-correlated, as was first observed by Peterson (1980) in M13.

To explore the presence of an anti-correlation between $[\text{Na}/\text{Fe}]$ and $[\text{O}/\text{Fe}]$ within our M71 sample as a whole, we construct Figure 27, which presents the Na versus O abundance diagram for our sample in M71. Our data are indicated by filled symbols, where triangles are red giants brighter than the HB, circles are HB stars, squares are red giants fainter than the HB and the stars near the main sequence turnoff are denoted by “stars”. Star-to-star Na variations and anti-correlation between Na and O abundances extend well beyond $M_V = +1.4$, and include the small sample of stars near the main sequence turnoff, where this anti-correlation has the same form as among the more luminous stars and is highly statistically significant at a level exceeding 4σ .

We find that Na and O are anti-correlated in our sample of M71 stars. The fit weighted by the error of Na vs. O, plotted as a solid line in Figure 27, is statistically significant at a 2σ confidence level.

Because of the large sample of bright RGB stars studied in M4 by Ivans *et al.* (1999), we adopt their results for the observed anti-correlation between Na and O among red giants in this cluster to provide a fiducial line for visual comparisons in the relevant figures. The anti-correlation found from their sample is indicated as a dashed line in Figure 27, as well as in the panels of Figure 28, to be discussed next. To within the errors, the Na/O anti-correlation we find in M71 agrees with that of M4, within a 2σ confidence level.

In Figure 28, we compare the determinations of Na and O abundance ratios that exist in the literature for metal poor globular clusters, 47 Tuc (Brown *et al.* 1990; Brown & Wallerstein 1992; Norris & DaCosta 1995), M71 (Snedden *et al.* 1994, , this paper), M5 (Ivans *et al.* 2001; Shetrone

1996; Sneden *et al.* 1992), M4 (Ivans *et al.* 1999), NGC 6752 (Gratton *et al.* 2001), M3 (Kraft *et al.* 1993), M10 (Kraft *et al.* 1995), M13 (Kraft *et al.* 1993; Shetrone 1996), NGC 6397 (Castilho *et al.* 2000; Gratton *et al.* 2001), M92 (Sneden *et al.* 1992), and M15 (Sneden *et al.* 1997). The symbols are the same as in Figure 27. Also included in this figure are the earlier results for ten bright giant stars in M71 from Sneden *et al.* (1994), shown in open triangles. All their stars are brighter than the HB and behave similarly to our red giants brighter than the HB. Our observed range in $[\text{Na}/\text{Fe}]$ is similar to the range observed by Sneden *et al.* (1994), but our range in $[\text{O}/\text{Fe}]$ is twice as big.

For each globular cluster depicted in Figure 28, the solid line represent the least squares linear fit of the data from the literature³. It is only shown for those globular clusters where the slope we derive is significant at the 2σ level. The dashed line corresponds to the anti-correlation observed in M4 from Ivans *et al.* (1999), shown as a fiducial line.

At this confidence level, we find Na-O anti-correlations in M71, M5, M4, NGC 6752, M3, M10, M13, M92 and M15. The steepest slope is that of M92, and the flattest slope is that of M13. But, within the 2σ level, all the slopes are identical. No statistically significant global anti-correlation is detected in 47 Tuc or NGC 6397.

47 Tuc ($[\text{Fe}/\text{H}] \sim -0.8$), M4 ($[\text{Fe}/\text{H}] \sim -1.2$) and NGC 6397 ($[\text{Fe}/\text{H}] \sim -2.0$) have a similar $[\text{Na}/\text{Fe}]$ versus $[\text{O}/\text{Fe}]$ relationship as does M71 does in terms of abundance ratio ranges and scatter. While the form of the relationship appears to be more or less universal, Figure 28 suggests that the amplitude of the Na/O anti-correlation among RGB stars is smallest for the two most metal rich globular clusters shown, 47 Tuc (where the published dataset is very small) and M71, as well as for NGC 6397.

4.5. Aluminium

The abundance of Al is also know to vary from star-to-star within a globular cluster. Because the Al doublet at 6697Å is not included in the spectral coverage of the primary set of HIRES spectra (see Paper I), it can be measured only in a subset of the sample of stars studied here. Our comparison between σ_{obs} and the predicted error of $[\text{Al}/\text{Fe}]$ given in Table 7 indicates that the scatter for this element abundance ratio is equal to its respective predicted error.

As discussed in §2.5, Al suffers from non-LTE effects. We have not adopted any corrections, nor have we applied any to the set of data from the literature assembled for Al. We do, however, use the 6696Å doublet, which is less susceptible to non-LTE effects than is the 3961Å line.

We have constructed Figure 29 to explore the presence of a correlation between $[\text{Na}/\text{Fe}]$ and

³Only for M71 do we use a fit weighted by the errors of each abundance determination; for all other clusters, the errors are assumed constant.

[Al/Fe] in M71, seen in other globular clusters. The symbols in Figure 29 are the same as in Figure 27. We include only our own data in this figure. A clear Al/Na anti-correlation is seen which is statistically significant at a level exceeding 2σ . This correlation extends down to $M_V = +1.8$ mag in M71, where the sample ends due to the technical issue of the HIRES spectral coverage.

In Figure 30, we compare the determinations of Al/Na abundance ratios that exist in the literature for metal poor globular clusters. We use the same set of references as in §4.4, although there are fewer stars with measured Al abundances. The symbols are the same as in Figure 27. Again the solid line, representing the least squares linear fit of the data, it is only shown in those globular clusters where the slope we derive is significant.

At the 2σ level, we find Na-Al correlations in M5, M4, NGC 6752, M13, NGC 6397, M92 and M15, as well as in M71. At this confidence level, all the slopes, with the exception of that of M13, are identical. No anti-correlation is detected in 47 Tuc, where the database is very sparse.

The differences among the family of linear fits to the Al/Na relationship for various globular clusters shown in Figure 30 appear at first sight to be considerably larger than those shown by the fits to the Na/O anti-correlation in Figure 28. We suggest that these differences may not be real, and may arise from non-LTE effects in Al acting on the different ranges of luminosities of stars studied in each cluster as well as the particular selection of Al lines used in each analysis. The situation in NGC 6752 is particularly illuminating. Gratton *et al.* (2001) ascribe the very different mean Al abundances deduced for the subgiants and for the main sequence stars in the cluster precisely to this issue of ignoring non-LTE in the spectrum of aluminium.

4.6. Lithium

Li is a very fragile element and is very easily destroyed in stars, burning at $T \gtrsim 2.5 \times 10^6$ K. Spite & Spite (1982) discovered the presence of Li in warm halo dwarfs at a constant value ($\log \epsilon(\text{Li}) = 2.24$) and suggested that this represents the primordial Li synthesized in the Big Bang, thus of considerable importance to cosmology. Destruction of Li is a measure of the depth of the surface convection zone, and hence a strong function of T_{eff} . Ryan *et al.* (2001) compile recent observations for Li in galactic disk and halo stars and review the Galactic chemical evolution of Li, while Pinsonneault (1997) reviews the destruction of Li from a theoretical perspective.

We therefore expect Li to be depleted among the RGB and subgiant stars in globular clusters, although probably not among the main sequence stars. In addition, there is at least one case known in a globular cluster of the extremely rare class of very Li-rich stars. A possible explanation for this star, found as a bright RGB star in M3 by Kraft *et al.* (1999), and similar objects is given by Charbonnel & Balachandran (2000).

The Li line is not included in the spectral coverage of the primary set of spectra (see Paper I), and hence can be measured only in a subset of the sample of M71 stars studied here. We were able

to obtain $\log \epsilon(\text{Li})$ for three giants fainter than the HB, as well as several upper limits. The mean $\log \epsilon(\text{Li})$ for the detections is 1.10 ± 0.16 (on the scale $H=12.0$ dex), which is 0.8 dex less than the mean $\log \epsilon(\text{Li})$ (1.90 ± 0.42) for a sample of 11 halo dwarf stars of similar $[\text{Fe}/\text{H}]$ from the sample of Fulbright (2000), and is evidence of the strong depletion among the cooler stars in which Li was detected here. Figure 2 illustrates the pattern of detections and upper limits, which are consistent with our overall expectations.

4.7. Carbon

The analysis of C I lines in cool stars is difficult as the lines are weak, and their excitation potential is high, ~ 8.5 eV. Furthermore, the C I lines near 7115\AA are not included in the spectral coverage of the primary set of spectra (see Paper I), and hence can be measured only in a subset of the sample studied here. We have reliable detections in only 6 stars, 2 lines in 1 star, and 1 line each in the other 5 stars. These, with considerable uncertainty, show a large star-to-star scatter in deduced C abundance. However, the C I lines in stars with $T_{\text{eff}} \lesssim 4200$ K may be blended with or completely dominated by lines from the red system of CN, as illustrated in the spectrum of Arcturus by Hinkle *et al.* (2000). It is very likely that this has happened, as there are two cool stars in our sample, M71 1-45 and 1-66, with anomalously high deduced C abundances. The measurements of Briley *et al.* (2001) show that these two stars have much stronger CN lines than does M71 star I, a star of similar T_{eff} which yielded a much more reasonable C abundance. Unpublished measurements of the G band of CH in these three stars also suggest that the very large C abundances we deduce for M71 1-45 and 1-66 are spurious.

The molecular band data gives a much clearer picture of the pattern of C abundance variation in M71 as the samples are much larger and the C abundance can be inferred with considerable precision from the strength of the CH band. Both the CH and CN bands clearly show strong star-to-star variations on the M71 giant branch (Briley *et al.* 2001, and references therein) and, more importantly, at the level of the main sequence (Cohen 1999). The entire set of molecular band data can be explained by a variation in C of about a factor of 2, with a much larger anti-correlated variation in the N abundance.

4.8. Other clusters

In Figures 31 to 34, for each element studied here we provide a comparison to similar high-resolution abundance analyses of halo dwarfs, of RGB stars in M4 ($[\text{Fe}/\text{H}] \sim -1.2$), RGB stars in M5 ($[\text{Fe}/\text{H}] \sim -1.2$), and RGB stars in M15 from Fulbright (2000), Ivans *et al.* (1999), Ivans *et al.* (2001), and Sneden *et al.* (1997), respectively. The halo dwarfs plotted in the Figures have been selected from the sample of Fulbright (2000) to have $[\text{Fe}/\text{H}]$ similar to M71 ($-0.6 < [\text{Fe}/\text{H}] < -0.9$). The boxes in Figures 31 to 34 follow the same layout as in Figure 24. The globular cluster name

is indicated above each box (‘H’ stands for the halo dwarf sample), and the number in parenthesis below the name indicates the number of stars used in the calculation of the respective abundance ratio.

The mean abundances for each element determined in each of the five different environments presented in Figures 31 to 34 agree to within the 1σ uncertainties of each measurement for most of the elements displayed, and agree to within $\pm 1.2\sigma$ for *all* the elements shown. Aluminium is the element showing the largest trend with metallicity between these five environments. This is perhaps a consequence of not considering non-LTE effects and of some studies including the 3961 Å doublet, known to be more sensitive to non-LTE effects, and others not. Barium is the only other element showing large variations in its mean abundance among the various environments, although no consistent trend with metallicity. We suggest that this too may not be real, and may be a reflection of the issue of hyperfine structure corrections in the fairly strong lines of this element.

Overall M71 appears to have very similar abundance ratios as does M5. In this set of figures, one can see some of the well known trends characteristic of halo star abundances as reviewed by McWilliam (1997), such as the gradual increase of $[\alpha/\text{Fe}]$ as $[\text{Fe}/\text{H}]$ decreases.

4.9. Interpretation

A classical review of post-main sequence stellar evolution can be found in Iben & Renzini (1983). Their description of the consequences of the first dredge up phase, the only dredge up phase any of the stars in our M71 sample may have experienced, indicates that a doubling of the surface N^{14} and a 30% reduction in the surface C^{12} can be expected, together with a drop in the ratio of $\text{C}^{12}/\text{C}^{13}$ from the solar value of 89 to ~ 20 , as well as a drop in surface Li and B by several orders of magnitude. Observations of field stars over a wide range of luminosities conform fairly well to this picture, see e.g. Shetrone *et al.* (1993); Gratton *et al.* (2000).

However, the O/Na anti-correlation seen among the bright red giants in many globular clusters, including here in the case of M71, cannot be explained in this picture. Several theoretical mechanisms have thus been proposed (e.g., the meridional mixing of Sweigart & Mengel (1979), and turbulent diffusion of Charbonnel (1994, 1995)) with varying degrees of success. In addition, Denisenkov & Denisenkova (1990) suggested that the nuclear reaction $^{22}\text{Ne}(p, \gamma)^{23}\text{Na}$ occurs in regions of the H-burning shell for low mass stars where O is converted into N and produces Na^{23} and Al^{27} . Langer *et al.* (1993) combined these ideas to predict the consequences of such possible synthesis and deep mixing, including for example, that the surface Mg abundance should be much less affected than that of Na or Al. These ideas form the basis of our current understanding of dredge up in low mass metal poor giants, with more recent calculations given by Denissenkov & Weiss (1996); Cavallo *et al.* (1998); Weiss *et al.* (2000), among others.

The clear prediction of this suite of calculations is that the earliest that deep mixing can begin is at the location of the bump in the luminosity function of the RGB which occurs when the

H-burning shell crosses a sharp chemical discontinuity. Zocalli *et al.* (1999) have shown that the luminosity of the RGB bump as a function of metallicity as determined from observation agrees well with that predicted by the theory of stellar evolution. Bono *et al.* (2001) further suggest that the agreement between the predicted luminosity function and actual star counts along the RGB in the vicinity of the bump in a suite of globular clusters is so good that mixing cannot have occurred any earlier, otherwise the evolutionary lifetimes, and hence the observed LF, of such stars would have been affected.

Our sample of M71 stars shows a statistically significant correlation between Al and Na abundances which extends to stars as faint as $M_V = +1.8$ mag. We also see an anti-correlation between the Na and O abundances extending down to near the main sequence turn off. We see variations in Li (as expected), and may see variations in Zr (not expected). Any variations in Mg are smaller than those of Al, Na or O (as expected). We know there are large anti-correlated C and N variations from the work of Cohen (1999); this too is expected.

The behavior of Li, which is very fragile and easily destroyed, is not controversial. It is, however, the range of luminosity over which the remainder of these variations are seen which is becoming more and more of a problem for any scenario which invokes dredge up and mixing. The Na/O anti-correlation we see in M71 extends to the main sequence turn off. The Al/Na correlation we see in M71 extends to at least as faint as $M_V = +1.8$, while the RGB bump in a cluster of the metallicity of M71 is at $M_V = +1.0$. Cohen (1999) has shown that the C/N anti-correlation extends to the stars at the main sequence turnoff and even fainter in M71. Briley & Cohen (2001) have shown that the C/N abundance range seen at the level of the main sequence is comparable to that seen among the bright red giants of M71 by many previous studies, the most recent of which is Briley *et al.* (2001).

The accumulated weight of recent evidence, both in M71 as described above and in other globular clusters such as 47 Tuc (see Cannon *et al.* 1998, and references therein) and NGC 6752 (see Gratton *et al.* 2001, and references therein), suggest that we are now back in the situation we were during the late 1980s. Unless we have missed some important aspect of stellar evolution with impact on mixing and dredge up, we must declare the mixing scenario a failure for the specific case of M71 (and several other globular clusters as well). Even the theoreticians in the forefront of this field are beginning to admit that deep mixing alone is not sufficient (Denissenkov & Weiss 2001; Ventura *et al.* 2001). Unless and until some major new concept relevant to this issue appears, we must now regard the fundamental origin of the star-to-star variations we see in M71 as arising outside the stars whose spectra we have studied here.

5. CONCLUSIONS

We present results of a high dispersion analysis of 22 elements to obtain abundance ratios for 25 members of the Galactic globular cluster M71. Our sample of stars includes 19 giant stars (9

of which are less luminous than the RHB), 3 horizontal branch stars, and 3 stars near the main sequence turnoff. Our conclusions are summarized as follows:

- The iron peak and neutron capture element abundance ratios show no trend with T_{eff} , and low scatter around the mean.
- The α -elements Mg, Ca, Si and Ti are overabundant relative to Fe. The scatter about the mean is small.
- An anti-correlation between the Na and O abundances for stars in M71 is detected with a statistical significance in excess of 2σ , and extends to the stars near the main sequence turn off.
- The [Na/Fe] versus [Al/Fe] correlation is detected with a statistical significance in excess of 2σ in our sample of M71 stars, and extends at least as faint as $M_V = +1.8$.
- Both extremely O poor, Na rich stars and extremely O rich, Na poor stars such as are observed in M5 and in M13 are not present in our sample of M71 stars.
- Li is varying among the subgiants (as expected), and Zr may be varying among the subgiants.

M71 appears very similar in its element abundance ratios to M5, which is not surprising as M5 has a metallicity only slightly lower, $[\text{Fe}/\text{H}] = -1.2$ dex (Ivans *et al.* 2001). However, the amplitude of the Na/O and Al/Na relationships appears to be somewhat larger in M5 than in M71, and still larger in even more metal poor clusters.

Our detailed abundance analysis of 25 stars in M71 has revealed abundance variations appearing at such low luminosities that deep mixing scenarios can no longer reproduce these results. This problem is made even more acute when we add in the data of Cohen (1999) and the analysis of Briley & Cohen (2001) of the CH and CN bands in M71. We are forced to the firm conclusion that much, if not all, of the abundance variations seen in M71 must have been in place before the present generation of stars we observe was formed, or (less likely) are the result of some type (binaries ?) of mass transfer.

In future papers, we will proceed to apply the techniques and analysis developed here for M71 to other more metal poor globular clusters, where the RGB bump is predicted to be somewhat more luminous and where, judging from the behavior of their bright RGB stars, we may anticipate finding even larger variations at low luminosities among the cluster subgiants and main sequence stars.

The entire Keck/HIRES user communities owes a huge debt to Jerry Nelson, Gerry Smith, Steve Vogt, and many other people who have worked to make the Keck Telescope and HIRES a reality and to operate and maintain the Keck Observatory. We are grateful to the W. M. Keck

Foundation for the vision to fund the construction of the W. M. Keck Observatory. The authors wish to extend special thanks to those of Hawaiian ancestry on whose sacred mountain we are privileged to be guests. Without their generous hospitality, none of the observations presented herein would have been possible. We are grateful to the National Science Foundation for partial support under grant AST-9819614 to JGC. We thank Jason Prochaska and Andy McWilliam for providing their tables of hyperfine structure in digital form.

REFERENCES

- Arp, H. C. & Hartwick, F. D. A., 1971, *ApJ*, 167, 499
- Anders, E. & Grevesse, N., 1989, *Geochim. Cosmochim. Acta*, 53, 197
- Baumüller, D. & Gehren, T., 1998, *A&A*, 307, 961
- Baumüller, D. & Gehren, T., 1997, *A&A*, 325, 1088
- Baumüller, D., Butler, K., & Gehren, T., 1998, *A&A*, 338, 637
- Biémont, E., Hibbert, A., Godefroid, M., Vaeck, N., & Fawcett, B. C., 1991, *ApJ*, 375, 818
- Bono, G., Cassisi, S., Zocalli, M. & Piotto, G., 2001, *ApJ*, 546, L109
- Briley, M. M. & Cohen, J. G., 2001, *AJ*, 122, 242
- Briley, M. M., Smith, G. H., & Claver, C. F., 2001, *AJ*, 122, 2561
- Brown J. A., Wallerstein, G., & Oke, J. B., 1990, *AJ*, 100, 1561
- Brown J. A. & Wallerstein, G., *AJ*, 104, 1818
- Burris, D. L., Pilachowski, C. A., Armandroff, T. E., Sneden, C., Cowan, J. J., & Roe, H., 2000, *ApJ*, 544, 302
- Cameron, A. G. W., 1982, *Ap.Sp.Sci.*, 82, 123
- Cannon, R. D., Croke, B. F. W., Bell, R. A., Hesser, J. E., & Stathakis, R. A., 1998, *MNRAS*, 298, 601
- Castilho, B. V., Pasquini, L., Allen, D. M., Barbuy, B., & Molaro, P., 2000, *A&A*, 361, 92
- Cavallo, R. M., Sweigart, A. V., & Bell, R. A., 1998, *ApJ*, 492, 575
- Charbonnel, C., 1994, *A&A*, 282, 811
- Charbonnel, C., 1995, *ApJ*, 453, L4
- Charbonnel, C. & Balachandran, S. C., 2000, *A&A*, 359, 563
- Cohen, J. G., 1983, *ApJ*, 270, 654
- Cohen, J. G., 1999, *AJ*, 117, 2434
- Cohen, J. G., Behr, B. B., & Briley, M. M., 2001, *AJ*, 122, 1420 (Paper I)
- de la Reza, R. & Muller, E.A., 1975, *Solar Physics*, 43, 15

- Denisenkov, P. A. & Denisenkova, S. N., SvAL, 16, 275
- Denissenkov, P. A. & Weiss, A., 1996, A&A, 308, 773
- Denissenkov, P. A. & Weiss, A., 2001, ApJ, 559, 115L
- Fuhr, J. R., Martin, G. A., & Wiese, W. L., 1988, J. Phys. Chem. Ref. Data 17, Suppl. 4
- Fulbright, J., 2000, ApJ, 120, 1841
- Gratton, R. G., Quarta, M. L., & Ortolani, S., 1986, A&A, 169, 208
- Gratton, R. G. & Sneden, C., 1994, A&A, 287, 927
- Gratton, R. G., Carretta, E., Eriksson, K., & Gustafsson, B., 1999, A&A, 350, 955
- Gratton, R.G., Sneden, C., Carretta, E. & Bragaglia, A., 2000, A&A, 354, 169
- Gratton, R. G., Bonifacio, P., Bragaglia, A., Carretta, E., Castellani, V., Centurion, M., Chieffi, A., Claudi, R., Clementini, G., D’Antona, F., Desidera, S., Francois, P., Grundahl, F., Lucatello, S., Molaro, P., Pasquini, L., Sneden, C., Spite, F., & Straniero, O., 2001, A&A, submitted
- Hinkle, K., Wallace, L., Valenti, J. & Harmer, D., 2000, *Visible and Near Infrared Atlas of the Arcturus Spectrum, 3727 – 9000 Å*, ASP Press, San Francisco
- Holweger, H., Bard, A., Kock, A., & Kock, M., 1991, A&A, 249, 545
- Iben, I. Jr. & Renzini, A., 1983, ARA&A, 21, 271
- Ivans, I. I., Sneden, C., Kraft, R. P., Suntzeff, N. B., Smith, V. V., Langer, G. E., & Fulbright, J. P., 1999, ApJ, 118, 1273
- Ivans, I. I., Kraft, R. P., Sneden, C., Smith, G., Rich, R. M., & Shetrone, M., 2001, ApJ, in press
- Johnson, J., 2002, ApJS, in press (astro-ph/0111181)
- Käppeler, F., Beer, H., & Wisshak, K., 1989, Rep.Prog.Phys., 52, 945
- Kraft, R. P., Sneden, C., Langer, G. E., & Shetrone, M. D., 1993, AJ, 106, 1490
- Kraft, R. P., 1994, PASP, 106, 553
- Kraft, R. P., Sneden, C., Langer, G. E., Shetrone, M. D., & Bolte, M., 1995, AJ, 109, 2586
- Kraft, R. P., Peterson, R. C., Puragra, G., Sneden, C., Fulbright, J. P., & Langer, G. E., 1999, ApJ, 518, L53
- Kurucz, R. L., 1993*a*, ATLAS9 Stellar Atmosphere Programs and 2 km/s Grid, (Kurucz CD-ROM No. 13)

- Kurucz, R. L., 1993*b*, SYNTHE Spectrum Synthesis Programs and Line Data (Kurucz CD-ROM No. 18)
- Langer, G. E., Hoffman, R. & Sneden, C., 1993, PASP, 105, 301
- Langer, G. E., & Hoffman, R. D., 1995, PASP, 107, 1177
- Langer, G. E., Hoffman, R. D., & Zaidins, C. S., 1997, PASP, 109, 244
- Leep, E. M., Oke, J. B., & Wallerstein, G., 1987, AJ, 93, 338
- Martin, G. A., Fuhr, J. R., & Wiese, W. L., 1988, J. Phys. Chem. Ref. Data 17, Suppl. 3
- McWilliam, A., 1997, ARA&A, 35, 503
- Meléndez, J., Barbuy, B., & Spite, F., 2001, ApJ, in press (astro-ph/0104184)
- Moore, C. E., Minnaert, M. G. J., & Houtgast, J., 1966, "The solar spectrum 2935 Å to 8770 Å", National Bureau of Standards Monograph, Washington: US Government Printing Office (USGPO).
- Norris & DaCosta, 1995, ApJ, 447, 680
- Peterson, R. C., 1980, ApJ, 237, 87
- Pinsonneault, M., 1997, ARA&A, 35, 557
- Prochaska, J. X., Naumov, S. O., Carney, B. W., McWilliam, A., & Wolfe, A. M., 2000, ApJ, 120, 2513
- Ramírez, S. V., Cohen, J. G., Buss, J., & Briley, M. M., 2001, AJ, 122, 1429
- Ryan, S. G., Kajino, T., Beers, T. C., Suzuki, T. K., Romano, D., Matteucci, F. & Rosolankova, K., 2001, ApJ, 545, 55
- Shetrone, M. D., 1996, AJ112, 1517
- Shetrone, M. D., Sneden, C. & Pilachowski, C. A., 1993, PASP, 105, 337
- Smith, G. & Raggett, D. St. J., 1981, J. Ph. B, 14, 4015
- Sneden, C., 1973, Ph.D. thesis, Univ. of Texas
- Sneden, C., Kraft, R. P., Langer, G. E., Prosser, C. F., & Shetrone, M. D., 1992, AJ, 104, 2121
- Sneden, C., Kraft, R. P., Langer, G. E., Prosser, C. F., & Shetrone, M. D., 1994, AJ, 107, 1773
- Sneden, C., Kraft, R. P., Langer, G. E., Prosser, C. F., & Shetrone, M. D., 1997, AJ, 114, 1964
- Sneden, C., Cowan, J. J. & Truran, J. W., 2001, Astro-ph/0101439

- Spite, F. & Spite, M., 1982, A&A, 115, 357
- Sweigart, A. V. & Mengel, J. G., 1979, ApJ, 229, 624
- Takeda, Y., Zhao, G., Chen, Y., Qiu, H., & Takada-Hidai, M., 2000, PASJ, submitted (astro-ph/0110165)
- Thévenin, F., 1989, A&AS, 77, 137
- Thévenin, F., 1990, A&AS, 82, 179
- Ventura, P., D’Antona, F., Mazzitelli, I. & Gratton, R., 2001, ApJ, 550, 65L
- Wallace, L., Hinkle, K. & Livingston, W.C., 1998, N.S.O. Technical Report 98-001, <http://ftp.noao.edu.fts/visatl/README>
- Weise, W. L., Smith, M. W., & Miles, B. M., 1969, Natl Stand. Ref. Data Ser., Natl Bur. Stand. (U.S.), NSRDS-NBS 22, Vol. II
- Weise, W. L., Fuhr, J. R., & Deters, T. M., 1996, J. Phys. Chem. Ref. Data Monograph No. 7
- Weiss, A., Denissenkov, P. A., & Charbonnel, C., 2000, A&A, 356, 181
- Zhao, G., Butler, K., & Gehren, T., 1998, A&A, 333, 219
- Zocalli, M., Cassisi, G., Piotto, G., Bono, G. & Salaris, M., 1999, ApJ, 518, L49

Table 1. Stellar Parameters for the M71 Sample from Paper II

ID ^a	T_{eff} (K)	$\log(g)$	ξ (km/s)
1-45	3950	0.90	1.46
I	4150	1.00	1.37
1-66	4250	1.35	1.32
1-64	4200	1.35	1.34
1-56	4525	1.60	1.19
1-95	4550	1.65	1.18
1-81	4550	1.75	1.18
1-1	4700	2.05	1.11
1-80 ^{b,c}	5300	2.45	1.61
1-87 ^b	5300	2.45	1.61
1-94 ^b	5300	2.45	1.61
1-60	4900	2.30	1.02
1-59	4600	2.30	1.16
G53476_4543	4900	2.65	1.02
2-160	5100	2.70	0.92
G53447_4707	5175	2.75	0.89
G53445_4647	5050	2.85	0.95
G53447_4703	5000	3.00	0.97
G53425_4612	5150	3.15	0.90
G53477_4539	5150	3.15	0.90
G53457_4709	5200	3.35	0.88
G53391_4628	5100	3.35	0.92
G53417_4431	5800	4.05	0.60
G53392_4624	5800	4.05	0.60
G53414_4435	5900	4.15	0.55

^aIdentifications are from Arp & Hartwick (1971) or are assigned based on the J2000 coordinates, rh rm rs.s dd dm dd becoming Grmrss_dmdd.

^bRHB star.

^cAppears to show rotation (Paper I).

Table 2. Equivalent Widths (mÅ)^a

Ion	$\lambda(\text{\AA})$	χ (eV)	$\log(gf)$	1–45	I	1–66	1–64	1–56	1–95	1–81	1–1	1–80	1–87	1–94	1–60
C I	7113.180	8.640	-0.773	35.5	16.1	38.4	30.0
C I	7115.170	8.640	-0.710	31.3
O I	6300.304	0.000	-9.780	76.2	73.8 ^b	57.1	71.6	42.4 ^b	44.9	44.5	30.5 ^b	18.8 ^b	23.4	20.1 ^b	30.4
O I	6363.776	0.020	-10.300	39.3	34.3	25.9	35.7	19.2 ^b	19.6	22.3	9.0 ^b	14.9 ^b
O I	7771.944	9.150	0.369	15.2 ^b	21.3	23.2 ^b	21.2	19.9	28.7	65.5	52.5	81.0	44.4
O I	7774.166	9.150	0.223	...	17.2 ^b	16.1 ^b	18.8 ^b	17.5 ^b	23.8	17.5 ^b	21.4 ^b	63.6	50.9	62.3 ^b	43.6 ^b
O I	7775.388	9.150	0.001	...	18.6	...	14.3 ^b	18.7 ^b	14.7 ^b	14.7 ^b	14.3 ^b	32.3	31.3	50.6 ^b	32.5
Na I	5682.633	2.100	-0.700	159.9	130.6	137.0	123.8 ^b	121.5	105.0	106.8	106.4	66.1 ^b	68.6	63.1	64.4 ^b
Na I	5688.193	2.100	-0.420	159.5	134.3	146.3	141.0	131.5	125.5	129.3	125.3	84.4	90.4	83.4	84.9 [§]
Na I	6154.225	2.100	-1.530	108.2	60.4	72.3	64.5	52.8	43.0	47.3	48.4	7.0 ^b	15.7 ^b	13.4 ^b	18.4 ^b
Na I	6160.747	2.100	-1.230	136.6	91.1 ^b	101.3	93.3	89.5	64.3	71.2	68.6	27.6	32.0	17.3	30.6 ^b
Mg I	5711.088	4.340	-1.670	137.7	139.4	136.0	126.3	128.1	126.3	124.1	103.9	100.1	102.2	97.9	107.3
Mg I	6318.717	5.110	-1.970	69.0	63.8	55.9	56.7	64.2	53.3	54.9	61.2	...	37.9	...	37.4
Mg I	6319.237	5.110	-2.220	55.9	51.0	50.2	53.9	...	38.7	43.1	26.9	25.3	...
Mg I	6319.495	5.110	-2.680
Mg I	6965.409	5.750	-1.870	35.7	34.9	41.8	40.8	...	37.6	42.5	31.3
Mg I	7193.184	5.750	-1.400	68.4	61.4	71.1	63.7	55.5	53.5	52.9	41.0	...	37.3
Mg I	7387.689	5.750	-0.870	51.3	66.9	62.2	54.4	...	52.9	61.4	48.8	...	51.6	41.6	...
Mg I	7657.603	5.110	-1.280	112.5	112.5	111.6	112.5	97.3	98.0	101.9	91.4	77.4	77.4
Mg I	7722.601	5.940	-1.800	35.6	32.8	46.8
Mg I	7930.810	5.940	-1.200	53.6	60.2	67.9	56.5	...	62.2	52.6	45.0

^aTable available electronically.^bLine identified by hand. All other lines are identified automatically.^cFe I line used in the $\lambda D - W_\lambda$ fit.

Table 3. Correction Factors for Inverted Solar gf Values

Ion	# Common Cines Between NIST & Solar	Correction Factor ^a (dex)
Mg I	4	+0.10
Al I	6	+0.21
Ca I	12	+0.33
Ti I	30	+0.05
Cr I	11	+0.05
Ni I	33	+0.05

^a $gf(\text{used}) = gf(\text{Thevenin}) + \text{Correction Factor}$

Table 4. Solar Abundance Ratios $[X/Fe]$

Ion	# lines	$[X/Fe]^a$ (dex)	σ^a (dex)	$\Delta[\text{our-meteoric}]^b$ (dex)
Li I ^c	1	0.94	...	-0.22 ^d
C I	4	+1.08	0.04	+0.03
O I	5	+1.53	0.10	+0.11
Na I	4	-1.30	0.09	-0.10
Mg I	10	+0.03	0.24	-0.05
Al I	6	-1.20	0.15	-0.17
Si I	20	+0.14	0.12	+0.09
K I	1	-2.28	...	+0.10
Ca I	15	-1.56	0.14	-0.39
Sc II	7	-4.26	0.12	+0.16
Ti I	40	-2.48	0.15	+0.09
V I	13	-3.55	0.14	-0.06
Cr I	12	-1.72	0.16	+0.10
Mn I	4	-2.09	0.12	-0.12
Co I	7	-2.60	0.08	0.00
Ni I	43	-1.19	0.18	+0.07
Cu I	1	-3.44	...	-0.20
Zn I	1	-2.88	...	-0.03
Y II	1	-4.96	...	+0.33
Zr I	4	-4.52	0.16	+0.38
Ba II	3	-5.29	0.08	+0.01
Eu II	1	-6.96	...	+0.01

^aMean and 1σ rms deviation about the mean for the abundance in the Sun of the lines of a particular ion using our adopted atomic line parameters.

^bMeteoric solar abundances from Anders & Grevesse (1989).

^c $\log \epsilon(\text{Li})$

^d $\Delta[\text{our-photospheric}]$, photospheric Li abundance from Anders & Grevesse (1989).

Table 5a. Abundance Ratios/Li–Na

Star	N _{Li}	log ϵ (Li) ^a	N _C	[C/Fe]	N _O	[O/Fe]	N _{Na}	[Na/Fe]
1–45	0	...	2	1.77±0.15	2	0.17±0.10	4	0.58±0.08
I	0	...	1	1.03±0.10	4	0.26±0.08	4	0.22±0.07
1–66	1	<−0.61	1	1.70±0.11	5	0.14±0.12	4	0.41±0.06
1–64	1	<−0.79	0	...	5	0.35±0.07	4	0.25±0.05
1–56	0	...	0	...	2	−0.07±0.11	4	0.30±0.07
1–95	1	<−0.39	1	1.14±0.09	4	0.13±0.14	4	0.21±0.06
1–81	0	...	0	...	4	0.22±0.08	4	0.24±0.06
1–1	1	<0.36	0	...	3	0.07±0.07	4	0.36±0.05
1–80	1	<−0.69	0	...	3	0.44±0.16	4	0.01±0.11
1–87	0	...	0	...	4	0.21±0.12	4	0.07±0.05
1–94	1	<−0.69	0	...	5	0.52±0.07	4	0.09±0.08
1–60	0	...	0	...	5	0.56±0.08	4	0.02±0.05
1–59	0	...	0	...	3	0.32±0.11	4	0.09±0.05
G53476_4543	0	...	0	...	5	0.24±0.12	4	0.13±0.05
2–160	1	<0.61	1	0.87±0.11	2	−0.16±0.13	3	0.30±0.06
G53447_4707	1	1.01±0.10	0	...	4	0.25±0.08	4	0.12±0.05
G53445_4647	1	0.99±0.10	1	0.57±0.09	4	0.15±0.13	4	0.13±0.05
G53447_4703	0	...	0	...	2	0.20±0.09	4	0.34±0.05
G53425_4612	1	1.29±0.10	0	...	3	0.23±0.07	4	0.19±0.08
G53477_4539	0	...	0	...	4	0.18±0.09	4	0.04±0.06
G53457_4709	0	...	0	...	2	0.19±0.07	4	0.08±0.06
G53391_4628	0	...	0	...	3	0.21±0.07	4	0.26±0.05
G53417_4431	0	...	0	...	3	−0.15±0.10	4	0.27±0.07
G53392_4624	0	...	0	...	3	0.08±0.07	3	0.17±0.09
G53414_4435	0	...	0	...	3	0.23±0.12	3	0.13±0.14

^alog ϵ (Li)=log(N_{Li}/N_H)+12, where N is number of atoms.

Table 5b. Abundance Ratios/Mg–Ca

Star	N _{Mg}	[Mg/Fe]	N _{Al}	[Al/Fe]	N _{Si}	[Si/Fe]	N _K	[K/Fe]	N _{Ca}	[Ca/Fe]
1–45	11	0.39±0.07	3	0.48±0.09	12	0.00±0.12	1	−0.67±0.09	15	0.38±0.07
I	12	0.38±0.06	3	0.30±0.11	14	0.24±0.08	1	−0.08±0.09	12	0.45±0.07
1–66	12	0.43±0.07	3	0.30±0.07	17	0.28±0.10	1	0.08±0.09	13	0.43±0.06
1–64	10	0.35±0.08	4	0.22±0.07	16	0.21±0.10	1	−0.78±0.09	15	0.44±0.06
1–56	4	0.27±0.07	0	...	10	0.39±0.15	0	...	10	0.42±0.07
1–95	13	0.37±0.07	3	0.14±0.07	17	0.40±0.06	1	−0.16±0.09	13	0.42±0.06
1–81	11	0.38±0.08	4	0.26±0.07	16	0.45±0.06	1	0.04±0.09	14	0.47±0.06
1–1	9	0.25±0.08	1	0.26±0.07	14	0.29±0.06	1	−0.05±0.09	12	0.54±0.06
1–80	2	0.31±0.06	0	...	10	0.47±0.06	0	...	9	0.45±0.12
1–87	7	0.27±0.07	0	...	16	0.45±0.06	0	...	12	0.45±0.08
1–94	4	0.34±0.10	2	0.08±0.07	13	0.40±0.06	1	−0.05±0.09	10	0.40±0.06
1–60	3	0.43±0.06	0	...	12	0.21±0.06	0	...	11	0.45±0.06
1–59	4	0.36±0.06	0	...	16	0.19±0.06	0	...	12	0.43±0.06
G53476_4543	5	0.31±0.06	0	...	18	0.29±0.06	0	...	15	0.41±0.06
2–160	9	0.23±0.07	2	0.15±0.07	17	0.45±0.09	0	...	13	0.45±0.06
G53447_4707	9	0.26±0.06	2	0.21±0.12	17	0.37±0.06	1	−0.24±0.09	12	0.46±0.06
G53445_4647	4	0.20±0.06	1	0.40±0.07	13	0.29±0.06	0	...	12	0.41±0.07
G53447_4703	4	0.33±0.08	0	...	16	0.24±0.06	1	0.15±0.09	13	0.34±0.06
G53425_4612	6	0.33±0.14	0	...	4	0.16±0.11	1	−0.04±0.09	9	0.44±0.06
G53477_4539	6	0.39±0.06	0	...	17	0.31±0.06	0	...	11	0.35±0.06
G53457_4709	4	0.41±0.11	0	...	11	0.12±0.12	0	...	11	0.46±0.07
G53391_4628	2	0.09±0.06	0	...	15	0.18±0.06	0	...	10	0.36±0.06
G53417_4431	1	0.11±0.06	0	...	5	0.00±0.13	0	...	11	0.37±0.06
G53392_4624	1	0.35±0.06	0	...	4	−0.04±0.12	0	...	8	0.33±0.07
G53414_4435	0	...	0	...	0	...	0	...	8	0.40±0.10

Table 5c. Abundance Ratios/Sc–Cr

Star	N _{Sc}	[Sc/Fe]	N _{Ti}	[Ti/Fe]	N _V	[V/Fe]	N _{Cr}	[Cr/Fe]
1–45	6	0.27±0.08	29	0.40±0.05	14	0.59±0.13	9	0.07±0.08
I	7	0.29±0.21	31	0.28±0.05	14	0.33±0.15	9	−0.01±0.07
1–66	6	0.23±0.07	33	0.30±0.04	13	0.19±0.07	9	0.00±0.07
1–64	7	0.21±0.12	33	0.34±0.04	14	0.35±0.15	8	0.00±0.07
1–56	4	−0.04±0.12	20	0.23±0.07	9	0.20±0.14	3	−0.14±0.11
1–95	6	0.14±0.06	36	0.16±0.04	14	0.13±0.08	9	−0.13±0.07
1–81	7	0.06±0.07	33	0.42±0.04	14	0.47±0.12	9	0.01±0.07
1–1	7	0.21±0.19	25	0.32±0.05	14	0.29±0.07	5	−0.06±0.07
1–80	4	−0.31±0.15	8	0.24±0.04	1	0.04±0.07	1	0.17±0.07
1–87	7	−0.13±0.06	16	0.20±0.04	10	0.28±0.07	4	−0.15±0.07
1–94	6	0.02±0.06	5	0.14±0.04	4	0.12±0.07	3	−0.28±0.10
1–60	5	0.21±0.07	10	0.11±0.06	3	−0.15±0.18	3	−0.11±0.15
1–59	5	0.26±0.06	23	0.21±0.04	11	0.16±0.07	7	−0.03±0.07
G53476_4543	6	0.15±0.06	32	0.28±0.04	11	0.25±0.07	9	−0.07±0.07
2–160	6	0.05±0.06	24	0.34±0.05	12	0.26±0.07	7	−0.01±0.08
G53447_4707	7	−0.04±0.07	21	0.24±0.04	9	0.20±0.07	8	−0.10±0.07
G53445_4647	7	0.01±0.06	15	0.28±0.04	8	0.27±0.08	6	−0.03±0.07
G53447_4703	7	0.30±0.21	17	0.28±0.04	6	0.15±0.08	6	0.02±0.07
G53425_4612	5	0.09±0.13	6	0.30±0.05	7	0.18±0.07	3	−0.08±0.13
G53477_4539	5	0.05±0.06	13	0.26±0.04	7	0.25±0.09	3	−0.14±0.14
G53457_4709	6	−0.03±0.06	8	0.31±0.04	3	0.20±0.07	3	−0.04±0.07
G53391_4628	6	0.13±0.06	15	0.38±0.04	0	...	3	−0.11±0.07
G53417_4431	3	−0.14±0.06	6	0.34±0.07	0	...	1	−0.09±0.07
G53392_4624	3	0.15±0.11	6	0.14±0.09	0	...	0	...
G53414_4435	1	0.20±0.06	4	0.23±0.16	0	...	0	...

Table 5d. Abundance Ratios/Mn–Zn

Star	N _{Mn}	[Mn/Fe]	N _{Co}	[Co/Fe]	N _{Ni}	[Ni/Fe]	N _{Cu}	[Cu/Fe]	N _{Zn}	[Zn/Fe]
1–45	3	−0.26±0.22	7	0.20±0.07	37	0.11±0.05	1	−0.10±0.09	0	...
I	4	−0.22±0.06	7	0.11±0.06	35	0.08±0.05	1	0.05±0.09	0	...
1–66	4	−0.22±0.06	7	0.12±0.05	35	0.10±0.06	1	0.15±0.09	1	0.73±0.12
1–64	4	−0.35±0.06	8	0.11±0.05	38	0.12±0.05	1	−0.21±0.09	1	0.63±0.12
1–56	0	...	3	0.09±0.05	29	0.08±0.06	0	...	0	...
1–95	4	−0.33±0.06	7	0.07±0.05	37	0.07±0.05	1	0.10±0.09	0	...
1–81	4	−0.15±0.06	7	0.11±0.05	36	0.04±0.05	1	0.11±0.09	0	...
1–1	4	−0.24±0.07	6	0.13±0.06	29	0.07±0.06	1	0.06±0.09	0	...
1–80	0	...	0	...	17	0.00±0.06	1	0.40±0.09	0	...
1–87	4	−0.21±0.08	4	0.21±0.08	27	−0.02±0.05	1	0.18±0.09	1	0.46±0.09
1–94	3	−0.28±0.06	0	...	16	0.05±0.06	1	0.13±0.09	1	0.44±0.09
1–60	0	...	2	0.14±0.13	19	0.04±0.05	1	−0.26±0.09	0	...
1–59	0	...	3	0.13±0.07	29	0.09±0.05	1	0.03±0.09	0	...
G53476_4543	0	...	3	0.15±0.05	36	0.03±0.05	1	0.08±0.09	0	...
2–160	3	−0.27±0.06	7	0.21±0.05	28	0.01±0.06	1	0.13±0.09	1	0.41±0.11
G53447_4707	3	−0.23±0.06	4	0.05±0.08	34	0.01±0.05	1	0.03±0.09	1	0.44±0.09
G53445_4647	0	...	2	0.09±0.16	23	0.04±0.07	1	0.20±0.09	1	0.34±0.09
G53447_4703	2	0.05±0.12	1	0.13±0.05	25	0.09±0.05	1	0.16±0.09	0	...
G53425_4612	2	−0.18±0.08	0	...	13	0.06±0.10	1	0.11±0.09	0	...
G53477_4539	0	...	0	...	24	0.01±0.06	1	0.12±0.09	0	...
G53457_4709	0	...	0	...	15	0.03±0.07	1	0.04±0.09	1	0.20±0.14
G53391_4628	0	...	2	0.24±0.15	21	0.04±0.07	1	0.19±0.09	0	...
G53417_4431	0	...	0	...	7	−0.06±0.14	0	...	0	...
G53392_4624	0	...	0	...	5	−0.16±0.15	0	...	0	...
G53414_4435	0	...	0	...	2	0.04±0.07	0	...	0	...

Table 5e. Abundance Ratios/Y-Eu

Star	N _Y	[Y/Fe]	N _{Zr}	[Zr/Fe]	N _{Ba}	[Ba/Fe]	N _{Eu}	[Eu/Fe]
1-45	0	...	3	0.26±0.26	3	0.36±0.15	1	0.64±0.09
I	1	-0.10±0.09	4	-0.09±0.09	3	0.43±0.08	1	0.48±0.09
1-66	0	...	4	-0.14±0.13	3	0.43±0.09	1	0.42±0.09
1-64	0	...	3	-0.07±0.08	2	0.41±0.08	1	0.52±0.09
1-56	0	...	1	-0.44±0.08	3	0.60±0.19	1	0.05±0.09
1-95	1	-0.22±0.09	3	-0.25±0.08	3	0.58±0.09	1	0.33±0.09
1-81	0	...	2	0.12±0.08	3	0.43±0.12	1	0.27±0.09
1-1	0	...	0	...	2	0.29±0.08	0	...
1-80	0	...	0	...	3	0.54±0.36	1	0.23±0.09
1-87	0	...	1	0.28±0.08	3	0.23±0.18	1	0.24±0.09
1-94	0	...	0	...	3	0.44±0.21	0	...
1-60	0	...	0	...	3	0.65±0.08	0	...
1-59	0	...	0	...	3	0.46±0.16	0	...
G53476_4543	0	...	1	-0.01±0.08	3	0.33±0.16	1	0.35±0.09
2-160	0	...	1	0.30±0.08	3	0.37±0.17	0	...
G53447_4707	1	-0.17±0.09	0	...	3	0.39±0.16	1	0.29±0.09
G53445_4647	0	...	0	...	2	0.44±0.20	0	...
G53447_4703	0	...	0	...	3	0.24±0.19	0	...
G53425_4612	0	...	0	...	3	0.51±0.10	0	...
G53477_4539	0	...	0	...	3	0.33±0.16	0	...
G53457_4709	0	...	0	...	3	0.32±0.19	0	...
G53391_4628	0	...	0	...	3	0.43±0.22	0	...
G53417_4431	0	...	0	...	3	0.35±0.13	0	...
G53392_4624	0	...	0	...	2	0.74±0.30	0	...
G53414_4435	0	...	0	...	3	0.47±0.08	0	...

Table 6. Sensitivity of Abundances

	ΔW_λ 10% ^a (dex)	ΔT_{eff} +100 K (dex)	$\Delta \log(g)$ +0.2 dex (dex)	$\Delta \xi$ +0.2 km s ⁻¹ (dex)	$\Delta [\text{Fe}/\text{H}]$ +0.2 dex (dex)
Li I :					
5000/2.5/1.0	0.10 ^b	0.13	0.01	0.00	0.01
C I :					
4000/1.0/1.4	0.00	-0.25	0.09	-0.02	0.02
4250/1.0/1.4	0.07	-0.17	0.09	-0.01	0.00
5000/2.5/1.0	0.07	-0.10	0.07	0.00	0.02
O I :					
4250/1.0/1.4	0.08	-0.19	0.09	-0.01	0.01
5000/2.5/1.0	0.08	-0.11	0.07	-0.01	0.02
5500/4.0/0.6	0.12	-0.08	0.05	0.00	0.02
[O I]:					
4250/1.0/1.4	0.06	0.02	0.08	-0.01	-0.07
5000/2.5/1.0	0.05	0.02	0.09	0.00	-0.06
Na I :					
4250/1.0/1.4	0.17	0.10	-0.02	-0.08	0.01
5000/2.5/1.0	0.10	0.08	-0.02	-0.03	0.01
5500/4.0/0.6	0.09	0.06	-0.02	-0.01	0.00
Mg I :					
4250/1.0/1.4	0.12	0.03	0.00	-0.04	-0.01
5000/2.5/1.0	0.10	0.06	-0.01	-0.03	0.01
5500/4.0/0.6	0.15	0.06	-0.03	-0.01	0.00
Al I :					
4250/1.0/1.4	0.08	0.08	-0.01	-0.03	0.01
5000/2.5/1.0	0.06	0.07	-0.01	-0.01	0.01
Si I :					
4000/1.0/1.4	0.09	-0.09	0.06	-0.03	-0.04
4250/1.0/1.4	0.09	-0.05	0.04	-0.03	-0.03
5000/2.5/1.0	0.08	0.02	0.01	-0.01	-0.01
5500/4.0/0.6	0.10	0.02	0.00	0.00	-0.01
K I :					

Table 6—Continued

	ΔW_λ 10% ^a (dex)	ΔT_{eff} +100 K (dex)	$\Delta \log(g)$ +0.2 dex (dex)	$\Delta \xi$ +0.2 km s ⁻¹ (dex)	$\Delta [\text{Fe}/\text{H}]$ +0.2 dex (dex)
4250/1.0/1.4	0.27	0.15	-0.02	-0.17	0.00
5000/2.5/0.6	0.28	0.12	-0.06	-0.08	-0.01
Ca I :					
4250/1.0/1.4	0.19	0.12	-0.03	-0.10	0.00
5000/2.5/1.0	0.14	0.09	-0.04	-0.05	0.00
5500/4.0/0.6	0.16	0.08	-0.06	-0.02	-0.01
Sc II:					
4250/1.0/1.4	0.31	-0.02	0.08	-0.12	-0.06
5000/2.5/1.0	0.19	0.00	0.08	-0.05	-0.06
5500/4.0/0.6	0.10	0.00	0.08	-0.01	-0.05
Ti I :					
4250/1.0/1.4	0.16	0.16	0.00	-0.09	0.01
5000/2.5/1.0	0.09	0.12	-0.01	-0.03	0.01
5500/4.0/0.6	0.09	0.10	-0.01	-0.01	0.01
V I :					
4250/1.0/1.4	0.40	0.19	0.01	-0.12	0.00
5000/2.5/1.0	0.16	0.15	-0.01	-0.02	0.01
Cr I :					
4250/1.0/1.4	0.14	0.11	0.00	-0.09	0.01
5000/2.5/1.0	0.08	0.09	-0.01	-0.03	0.01
Mn I :					
4250/1.0/1.4	0.41	0.10	0.01	-0.07	-0.01
5000/2.5/1.0	0.26	0.10	-0.01	-0.03	0.01
Fe I :					
4250/1.0/1.4	0.15	0.04	0.02	-0.09	-0.03
5000/2.5/1.0	0.12	0.09	-0.01	-0.06	0.00
5500/4.0/0.6	0.14	0.08	-0.02	-0.03	0.00
Fe II:					
4000/1.0/1.4	0.09	-0.17	0.12	-0.04	-0.08
4250/1.0/1.4	0.09	-0.12	0.11	-0.04	-0.07

Table 6—Continued

	ΔW_λ 10% ^a (dex)	ΔT_{eff} +100 K (dex)	$\Delta \log(g)$ +0.2 dex (dex)	$\Delta \xi$ +0.2 km s ⁻¹ (dex)	$\Delta [\text{Fe}/\text{H}]$ +0.2 dex (dex)
5000/2.5/1.0	0.08	-0.04	0.09	-0.03	-0.04
5500/4.0/0.6	0.12	-0.03	0.08	-0.02	-0.04
Co I :					
4250/1.0/1.4	0.22	0.06	0.04	-0.01	-0.04
5000/2.5/1.0	0.09	0.11	0.01	0.00	-0.01
Ni I :					
4250/1.0/1.4	0.16	0.02	0.04	-0.10	-0.04
5000/2.5/1.0	0.11	0.07	0.01	-0.05	-0.01
5500/4.0/0.6	0.12	0.06	0.00	-0.03	-0.01
Cu I :					
4250/1.0/1.4	0.38	0.07	0.05	-0.10	-0.03
5000/2.5/1.0	0.34	0.11	0.01	-0.03	0.00
Zn I :					
4250/1.0/1.4	0.05	-0.02	0.05	-0.01	-0.02
Y II :					
4250/1.0/1.4	0.07	-0.03	0.09	-0.03	-0.07
Zr I :					
4250/1.0/1.4	0.13	0.21	0.01	-0.09	0.01
5000/2.5/1.0	0.05	0.16	-0.01	-0.01	0.01
Ba II:					
4250/1.0/1.4	0.35	0.02	0.06	-0.19	-0.09
5000/2.5/1.0	0.29	0.03	0.04	-0.16	-0.08
5500/4.0/0.6	0.21	0.04	0.02	-0.09	-0.07
Eu II:					
4250/1.0/1.4	0.09	-0.02	0.08	-0.06	-0.07
5000/2.5/1.0	0.05	0.00	0.07	-0.02	-0.06

^a15% for lines with hyperfine structure splitting and the ones of the 8 most faintest stars

^bEstimated error in the synthesis

Table 7. Mean Abundance Ratios and Errors

	# stars	$\langle [X/Fe] \rangle$ (dex)	σ_{obs} (dex)	σ_{pred} (dex)	Δ_{max} (dex)
Li ^a	3	+1.10	0.17	0.13	...
C	6	+1.07 ^b	0.44 ^b	0.11	0.88 ± 0.34^b
O	25	+0.22	0.17	0.13	0.10 ± 0.13
Na	25	+0.20	0.13	0.10	0.29 ± 0.13
Mg	24	+0.31	0.09	0.12	0.17 ± 0.07
Al	11	+0.25	0.11	0.10	0.17 ± 0.10
Si	24	+0.30	0.15	0.12	0.06 ± 0.12
K	11	−0.16	0.28	0.30	0.42 ± 0.25
Ca	25	+0.42	0.05	0.11	0.07 ± 0.04
Sc	25	+0.08	0.15	0.16	0.27 ± 0.09
Ti	25	+0.27	0.08	0.12	0.11 ± 0.07
V	21	+0.21	0.15	0.22	0.14 ± 0.08
Cr	23	−0.04	0.09	0.09	0.10 ± 0.07
Mn	13	−0.24	0.10	0.20	0.04 ± 0.07
Co	17	+0.13	0.05	0.11	0.05 ± 0.04
Ni	25	+0.05	0.06	0.09	0.14 ± 0.02
Cu	21	+0.08	0.14	0.37	0.22 ± 0.09
Zn	8	+0.45	0.15	0.13	0.28 ± 0.10
Y	3	−0.16	0.05	0.15	0.06 ± 0.11
Zr	10	−0.02	0.23	0.15	0.50 ± 0.23
Ba	25	+0.44	0.12	0.22	0.02 ± 0.08
Eu	11	+0.35	0.15	0.15	0.30 ± 0.11

^aFor Li, $\log \epsilon(\text{Li})$ (H=12.0 dex) is given. For all other elements, $[X/Fe]$ is given.

^bThe C abundances determined from C I lines in the cooler M71 stars are believed to be spurious due to contamination by lines from the red system of CN.

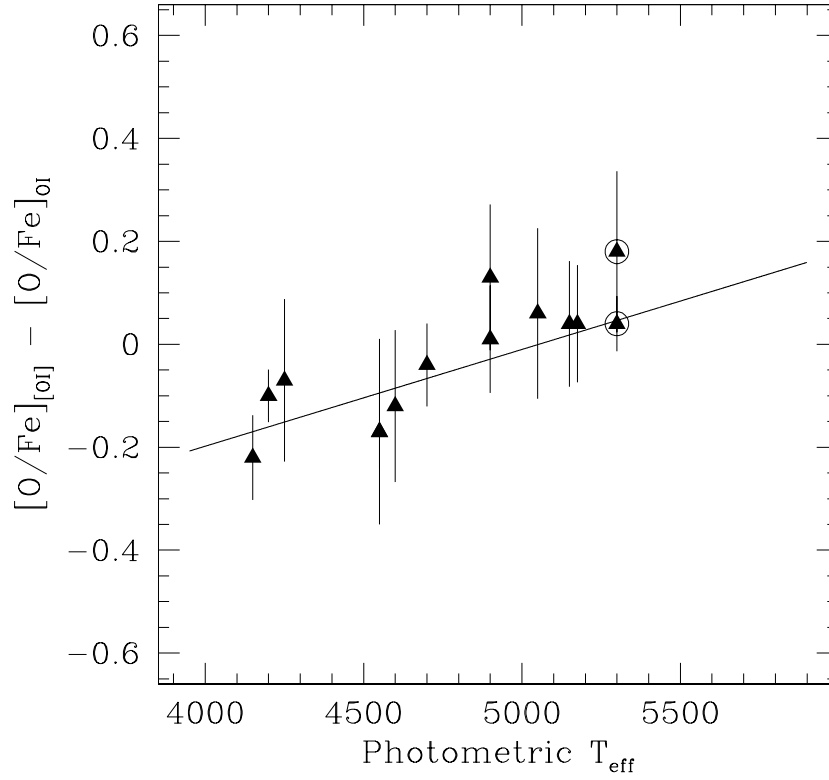


Fig. 1.— The difference between the oxygen abundance ratio from the forbidden and permitted lines is shown as a function of T_{eff} . The solid line is a linear fit weighted by the errors. The O abundances subsequently deduced from the permitted lines are corrected by the linear fit shown here. The RHB stars are marked with open circles.

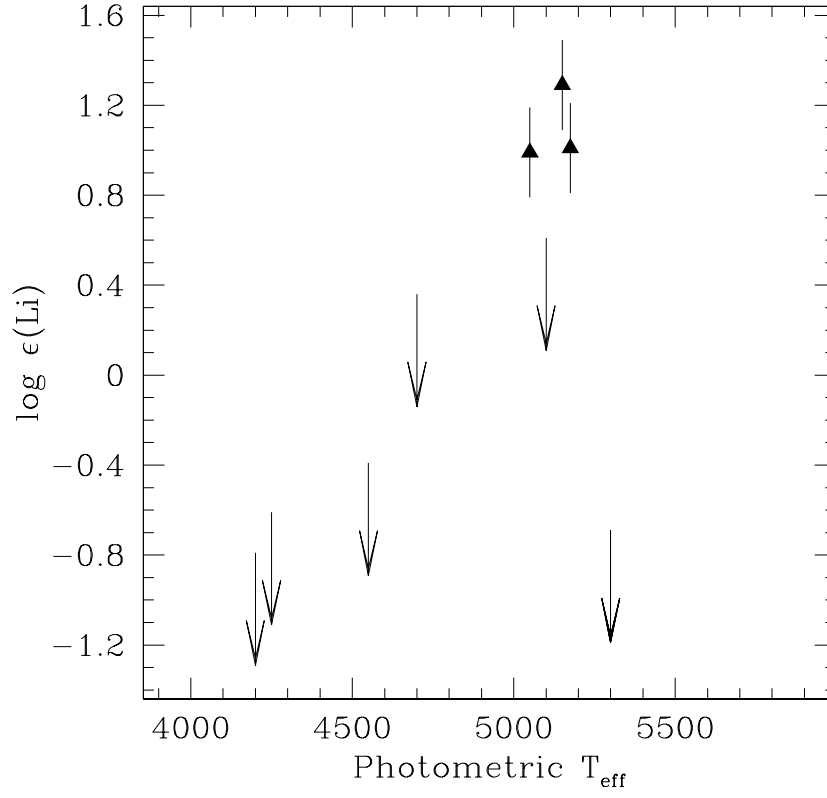


Fig. 2.— $\log \epsilon(\text{Li})$ against T_{eff} . The RHB stars are marked by open circles. Arrows represent upper limits for the strength of the Li I line.

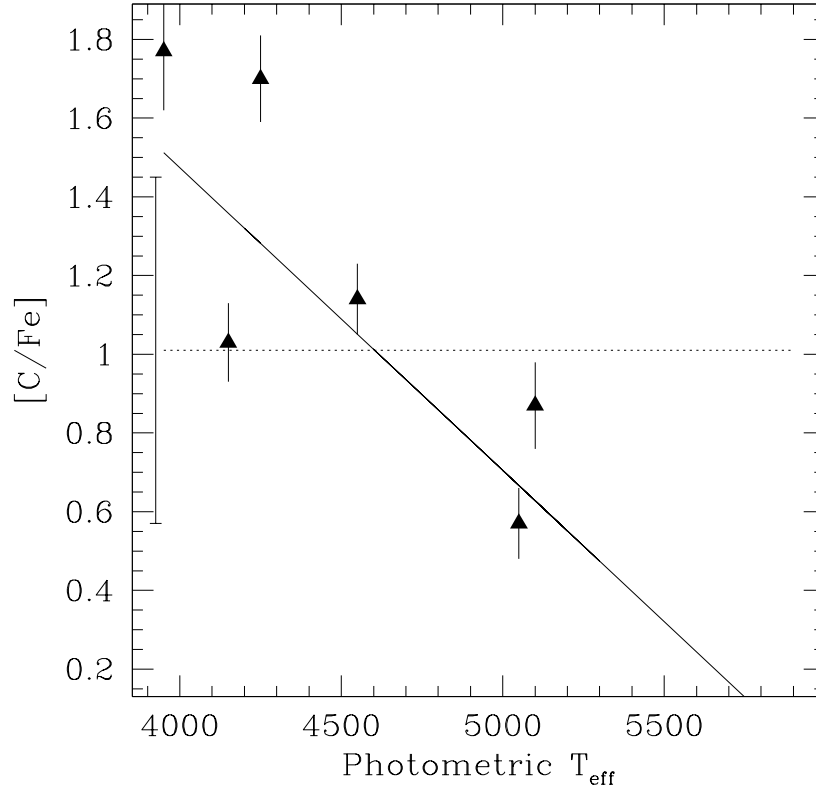


Fig. 3.— $[C/Fe]$ against T_{eff} . The solid line is a linear fit weighted by the errors. The dashed line indicates the mean abundance ratio with its respective error plotted as an error bar at 3925 K. The C abundances determined from C I lines in the cooler M71 stars are believed to be spurious due to contamination by lines from the red system of CN (see text).

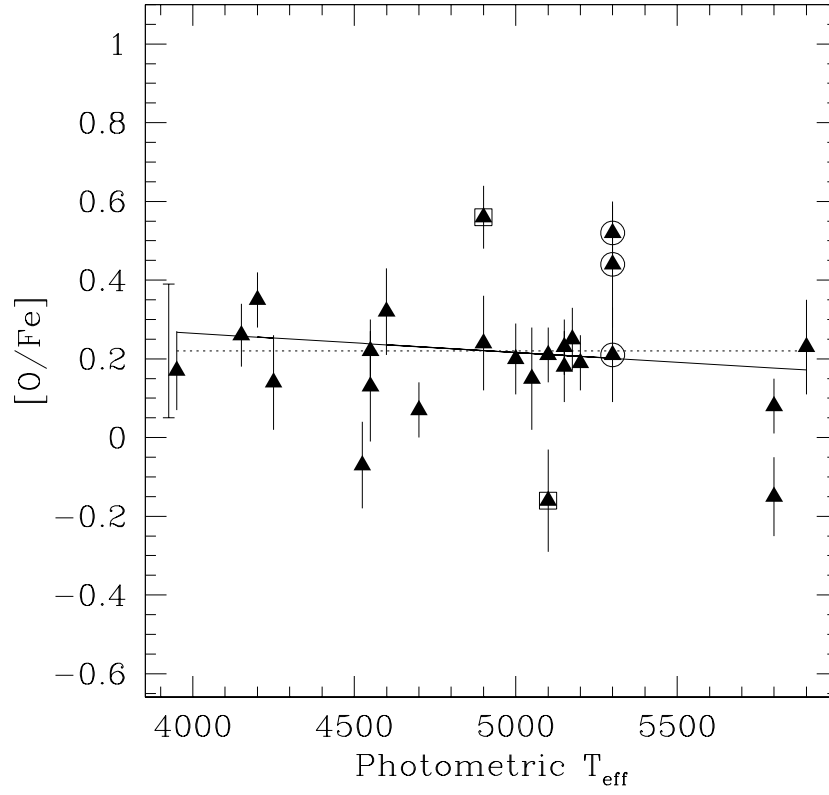


Fig. 4.— $[O/Fe]$ against T_{eff} . The solid line is a linear fit weighted by the errors. The dashed line indicates the mean abundance ratio with its respective error plotted as an error bar at 3925 K. The RHB stars are marked by open circles. Stars 1–60 and 2–160, which represent the extremes of the O abundance in our M71 sample, are marked with open squares.

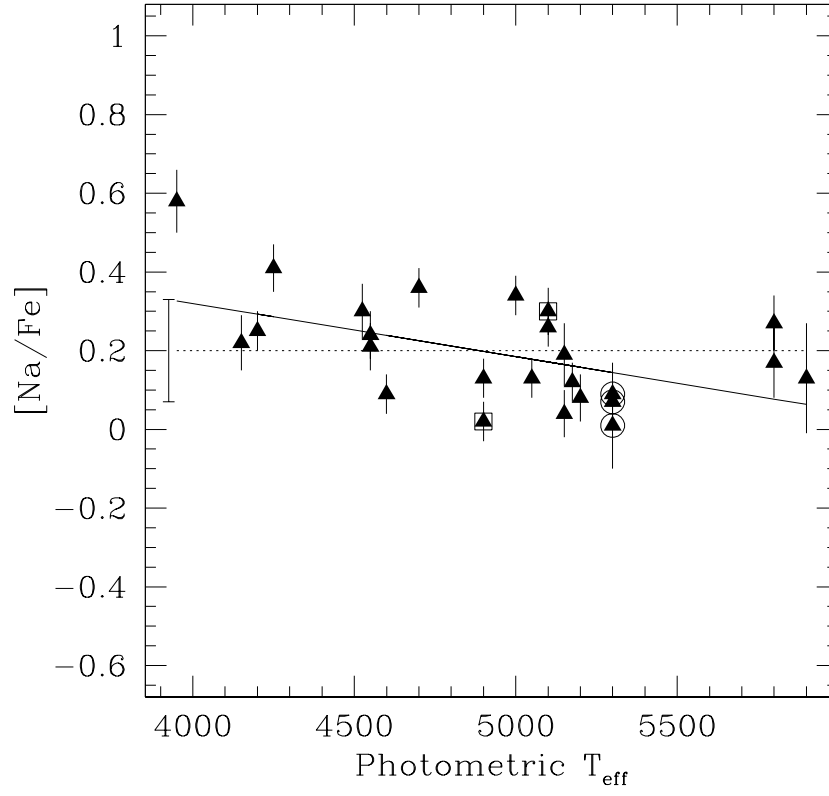


Fig. 5.— $[Na/Fe]$ against T_{eff} . The symbols are the same as in Figure 4. Stars 1–60 and 2–160, which represent the extremes of the O abundance in the M71 sample, are marked with open squares.

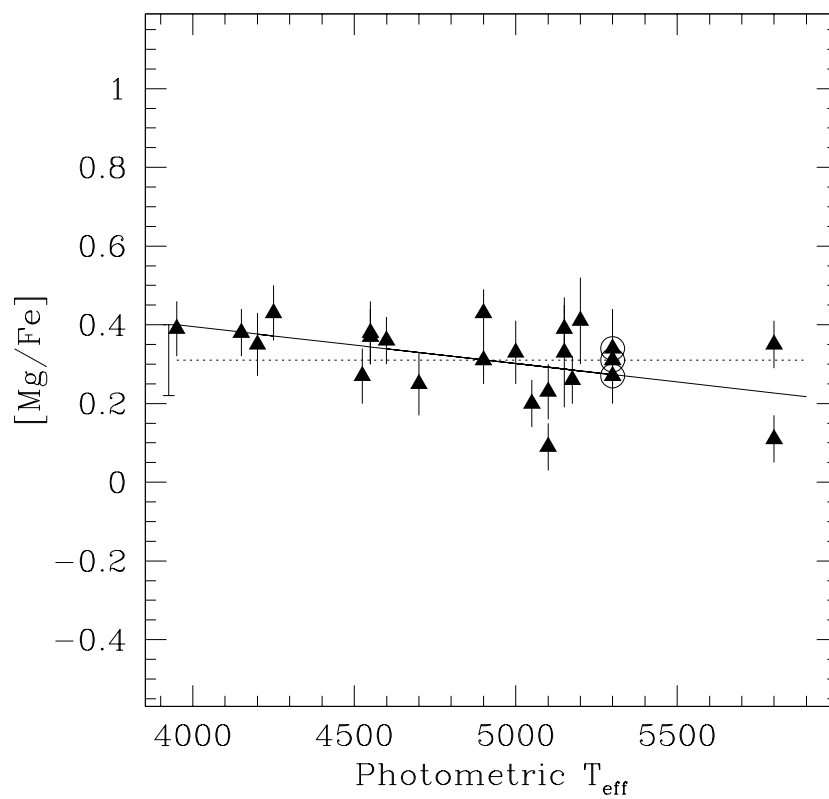


Fig. 6.— $[Mg/Fe]$ against T_{eff} . The symbols are the same as in Figure 4.

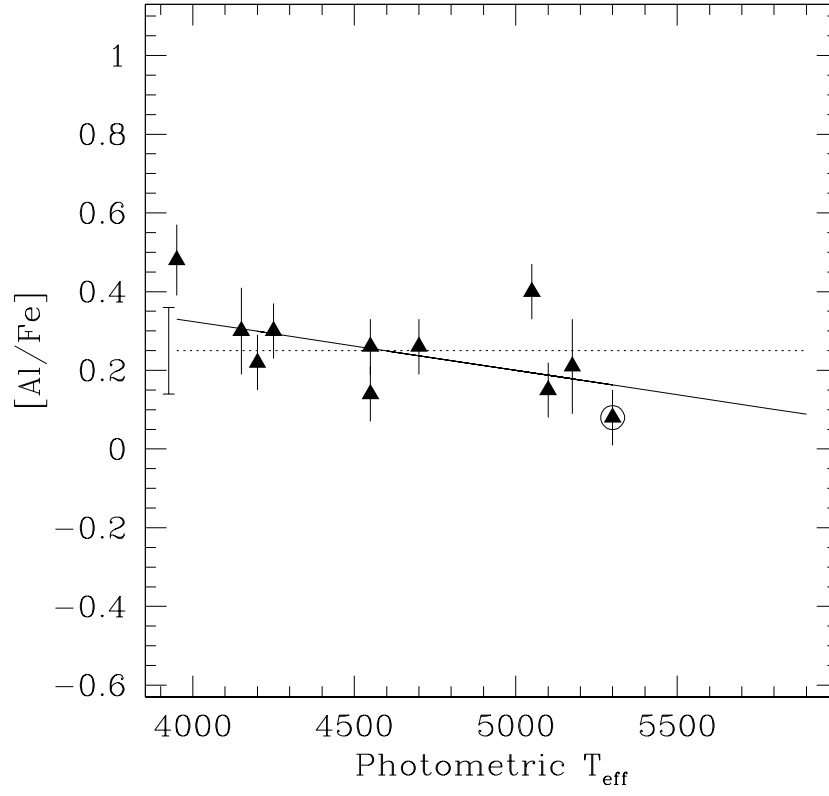


Fig. 7.— $[Al/Fe]$ against T_{eff} . The symbols are the same as in Figure 4. No correction for non-LTE has been applied.

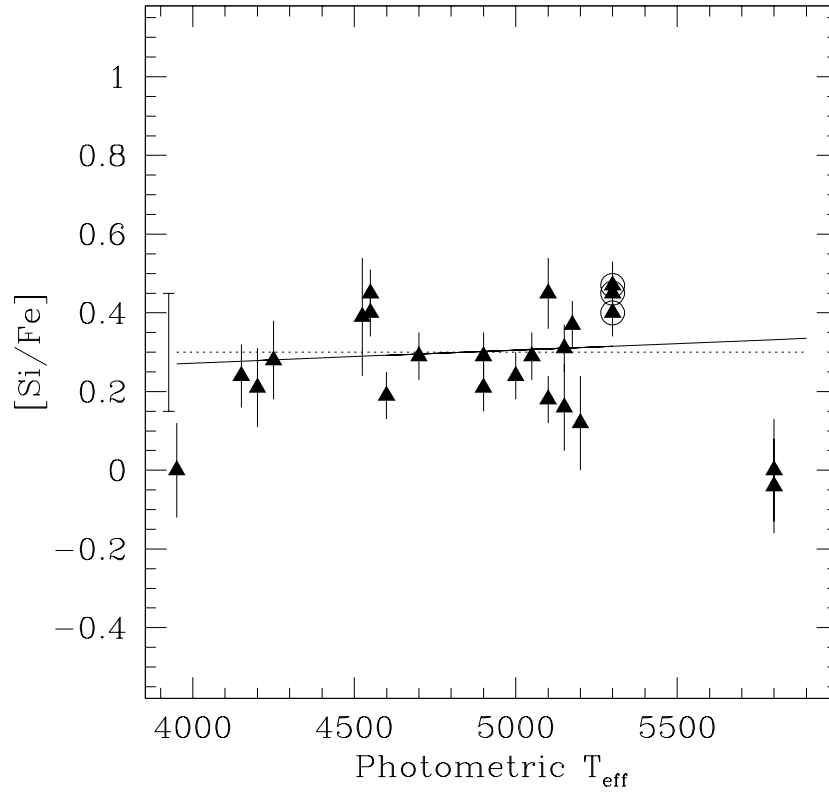


Fig. 8.— $[\text{Si}/\text{Fe}]$ against T_{eff} . The symbols are the same as in Figure 4.

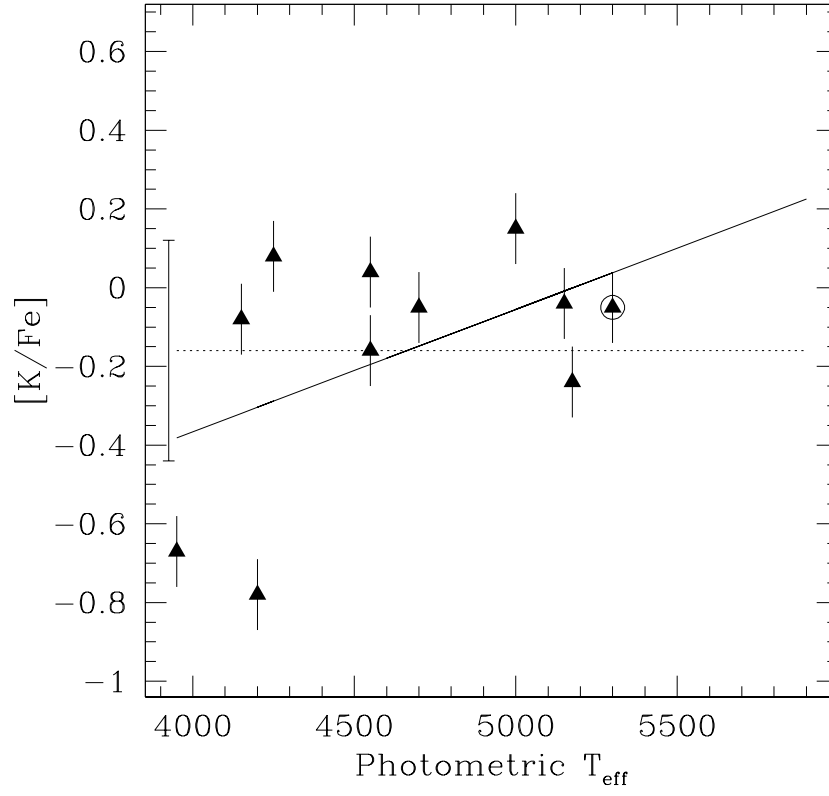


Fig. 9.— $[K/Fe]$ against T_{eff} . The symbols are the same as in Figure 4. A non-LTE correction has been applied.

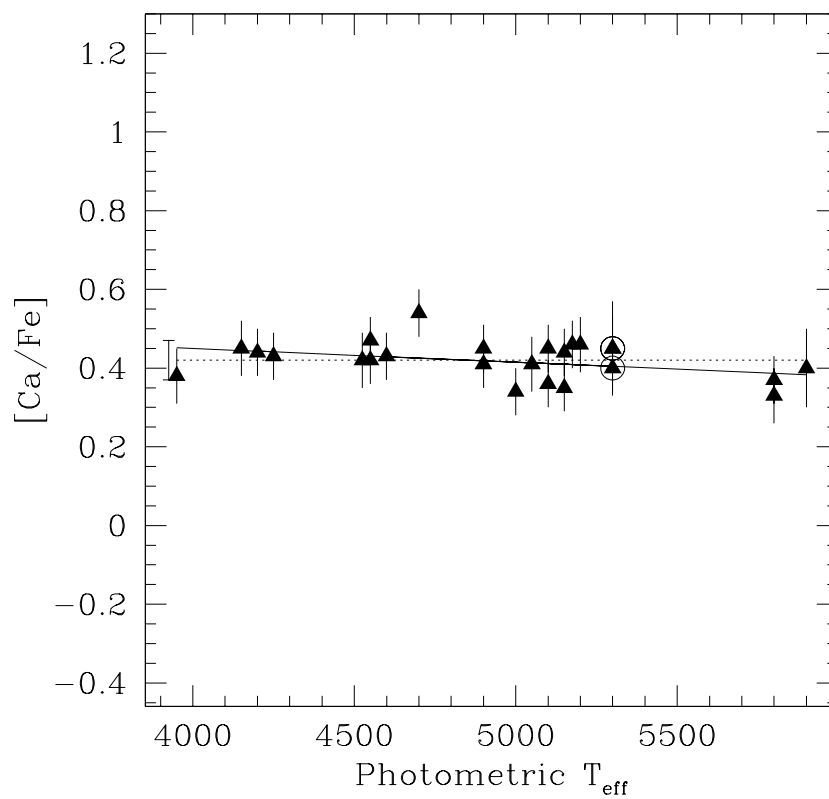


Fig. 10.— $[Ca/Fe]$ against T_{eff} . The symbols are the same as in Figure 4.

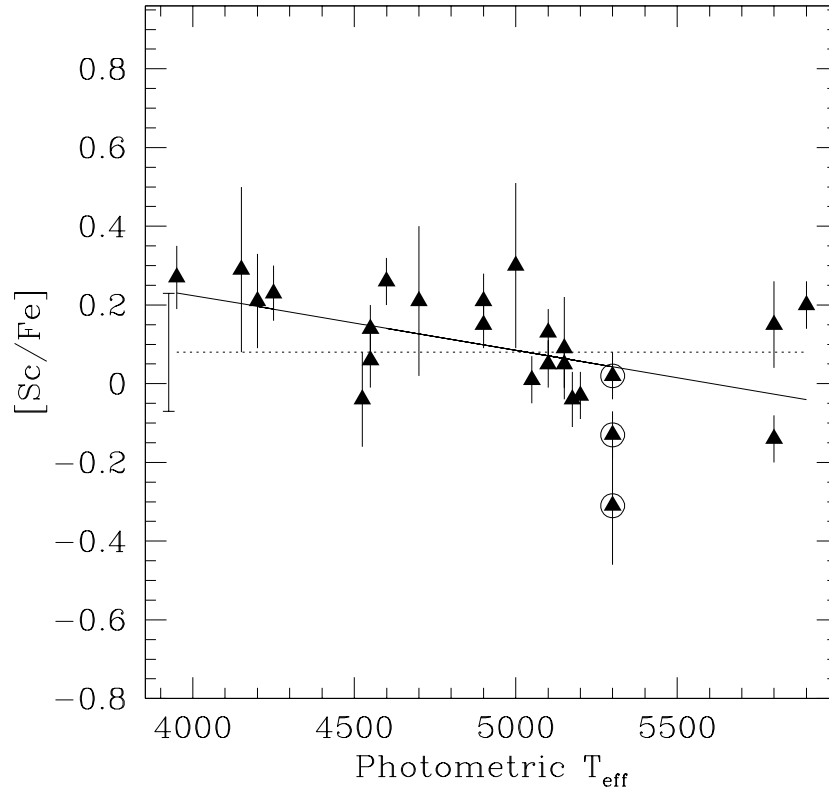


Fig. 11.— $[\text{Sc}/\text{Fe}]$ against T_{eff} . The symbols are the same as in Figure 4.

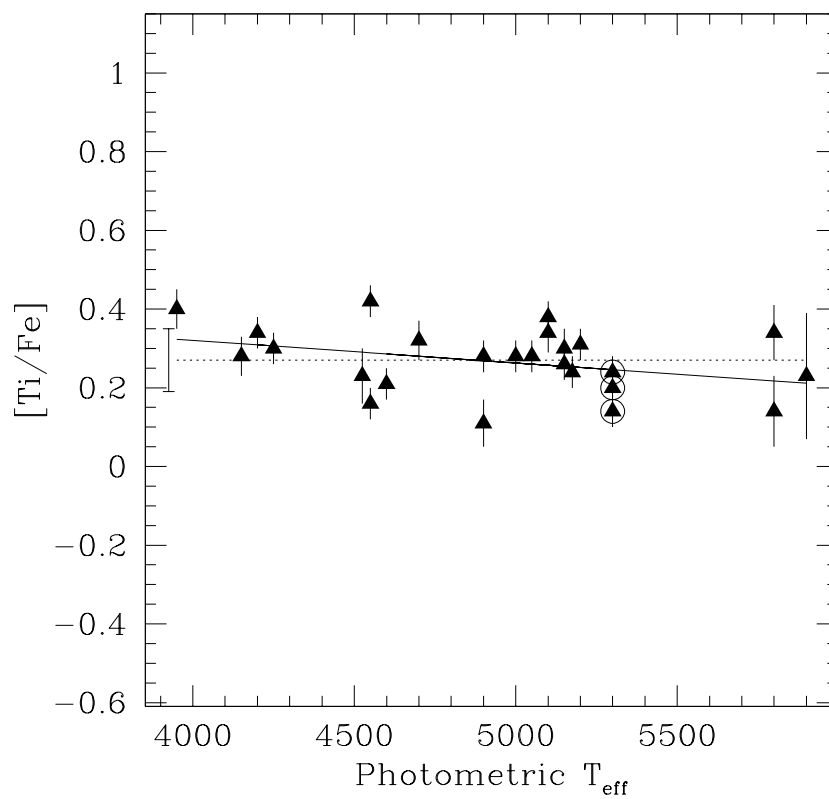


Fig. 12.— [Ti/Fe] against T_{eff} . The symbols are the same as in Figure 4.

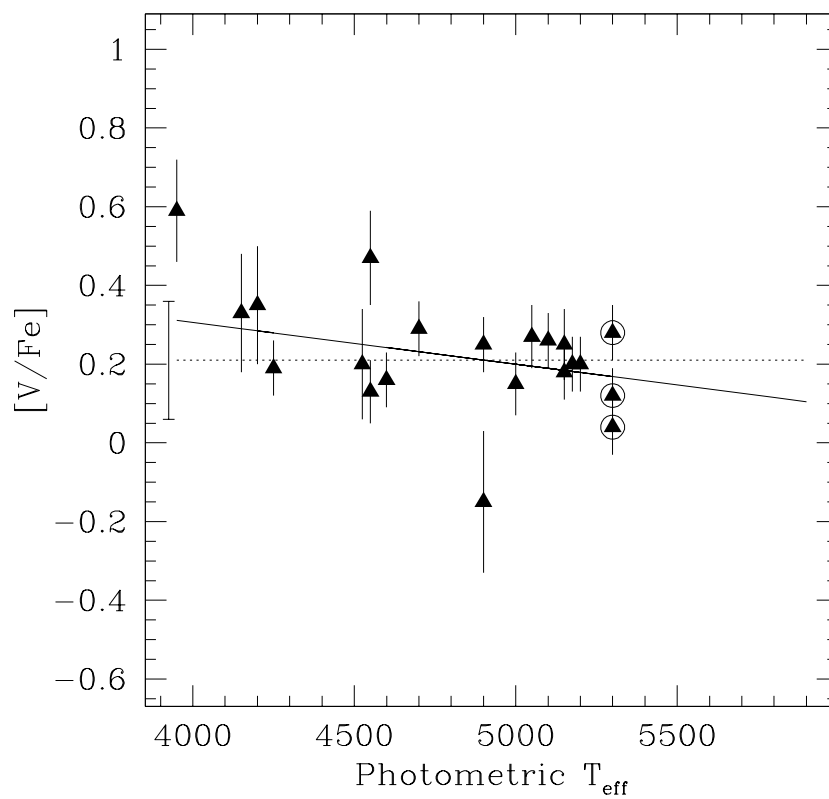


Fig. 13.— $[V/Fe]$ against T_{eff} . The symbols are the same as in Figure 4.

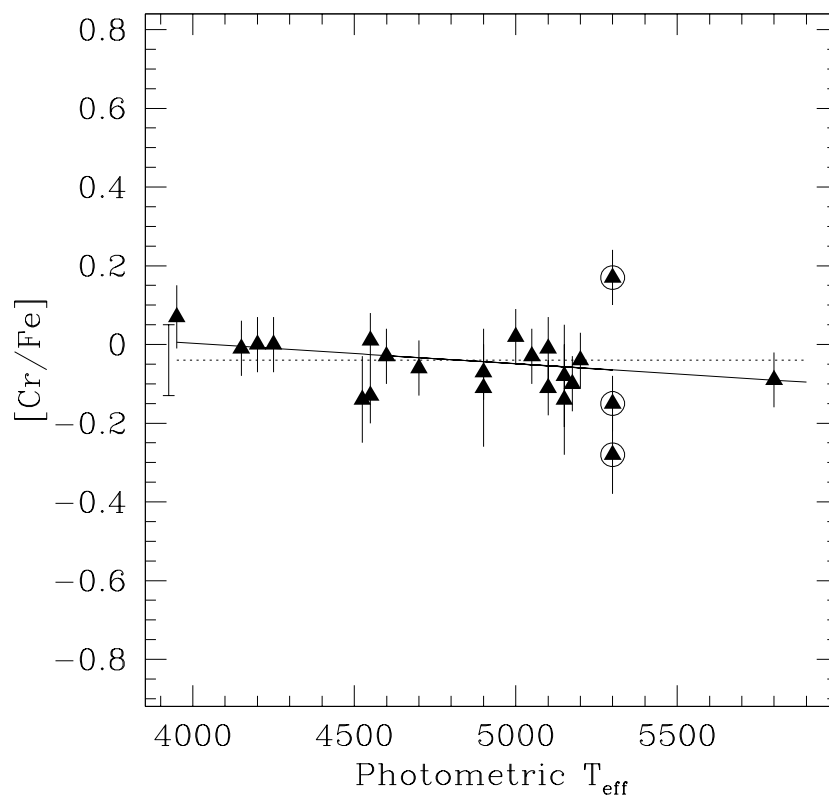


Fig. 14.— $[\text{Cr}/\text{Fe}]$ against T_{eff} . The symbols are the same as in Figure 4.

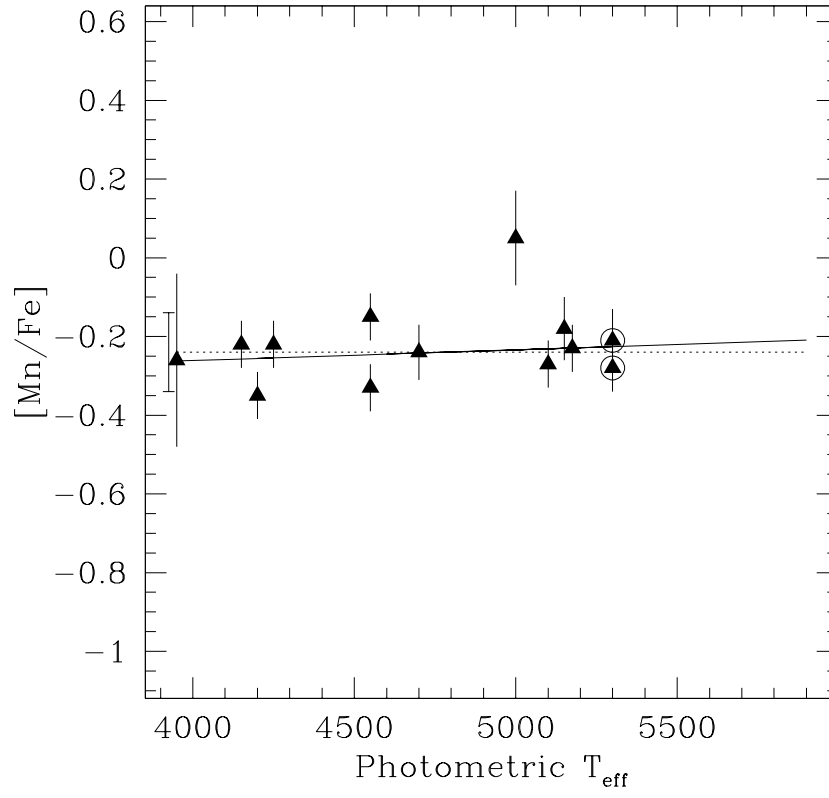


Fig. 15.— $[Mn/Fe]$ against T_{eff} . The symbols are the same as in Figure 4.

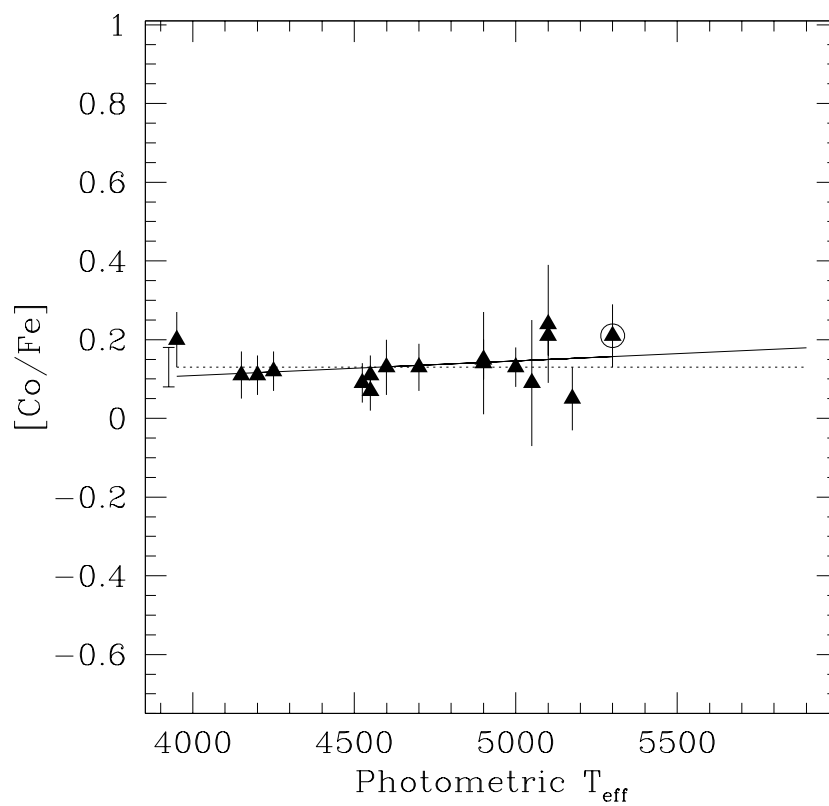


Fig. 16.— $[\text{Co}/\text{Fe}]$ against T_{eff} . The symbols are the same as in Figure 4.

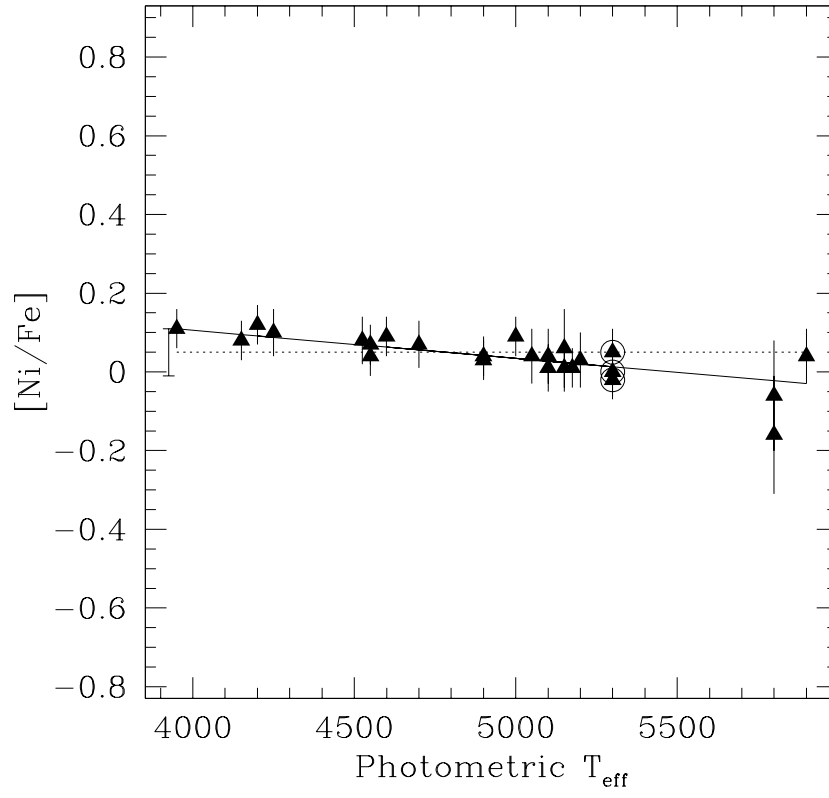


Fig. 17.— $[\text{Ni}/\text{Fe}]$ against T_{eff} . The symbols are the same as in Figure 4.

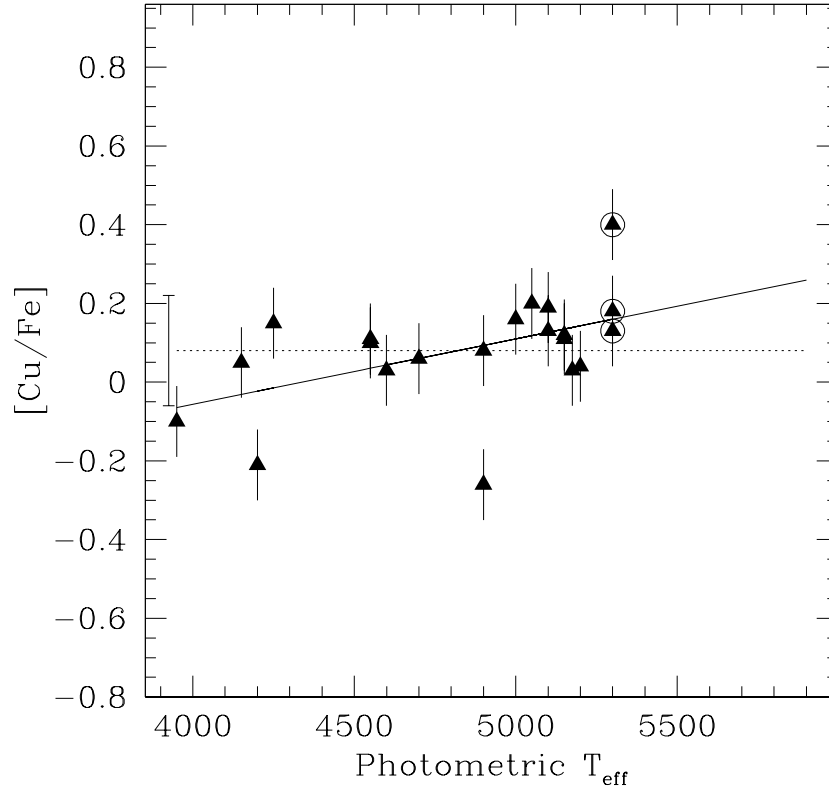


Fig. 18.— $[\text{Cu}/\text{Fe}]$, based on a single line with hyperfine structure, against T_{eff} . The symbols are the same as in Figure 4.

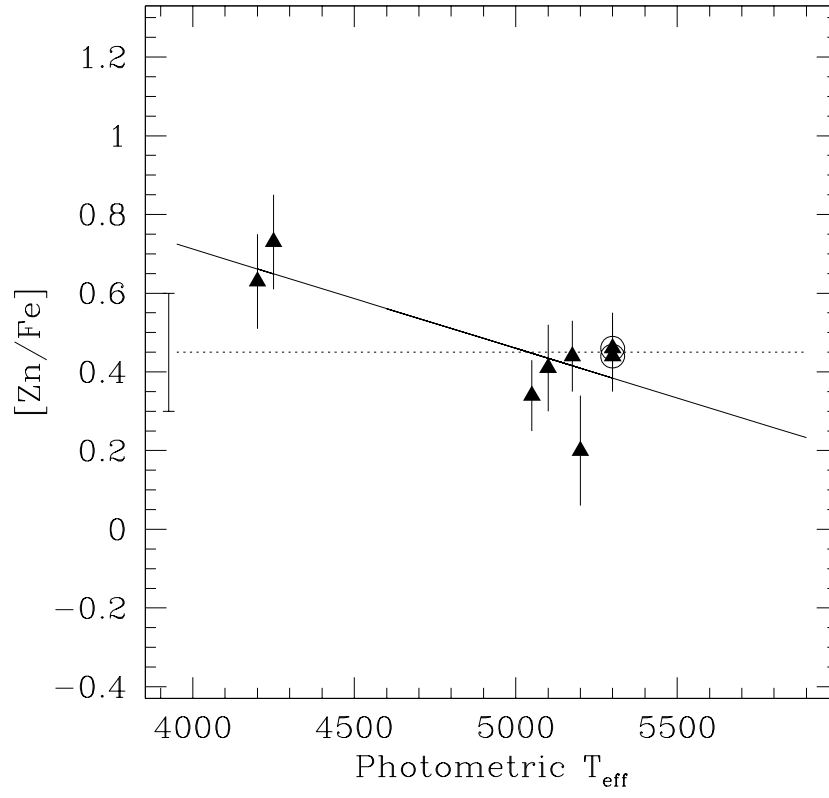


Fig. 19.— $[Zn/Fe]$, based on a single line, against T_{eff} . The symbols are the same as in Figure 4.

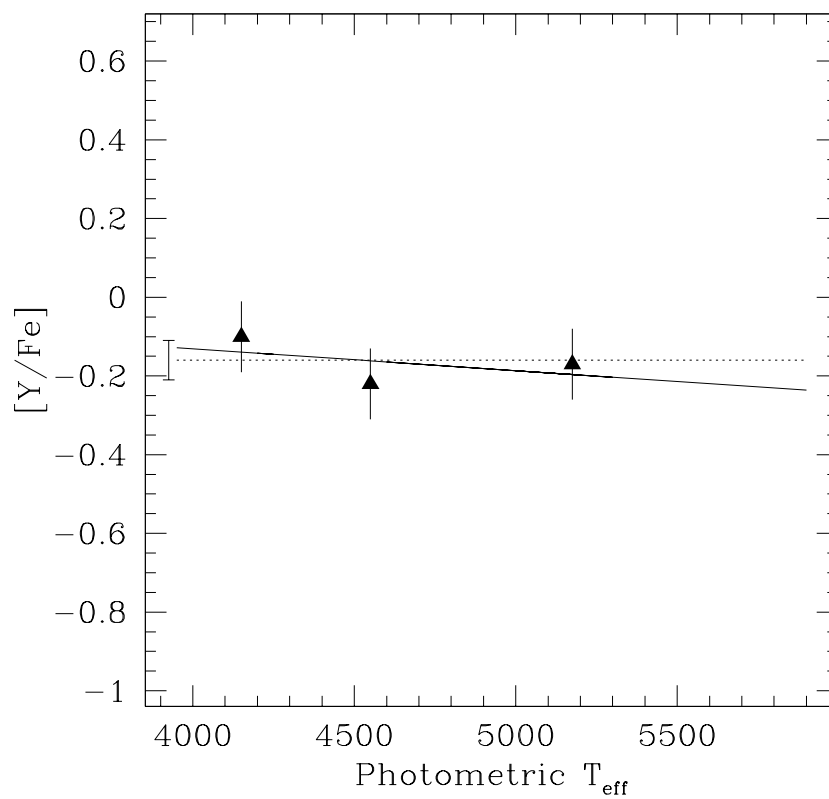


Fig. 20.— $[Y/Fe]$ against T_{eff} . The symbols are the same as in Figure 4.

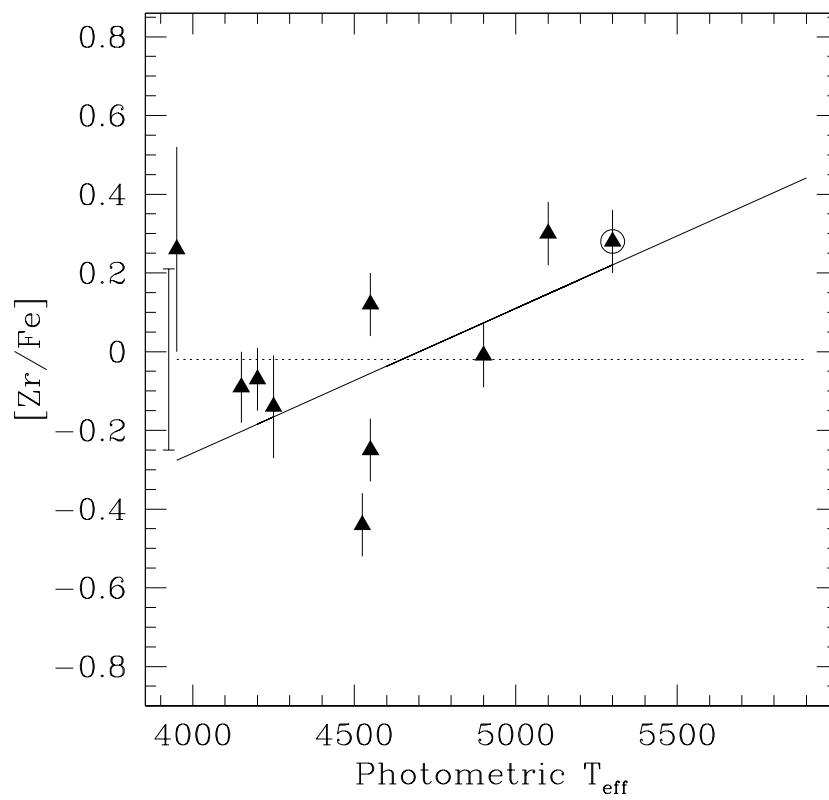


Fig. 21.— [Zr/Fe] against T_{eff} . The symbols are the same as in Figure 4. Note the unusually large scatter.

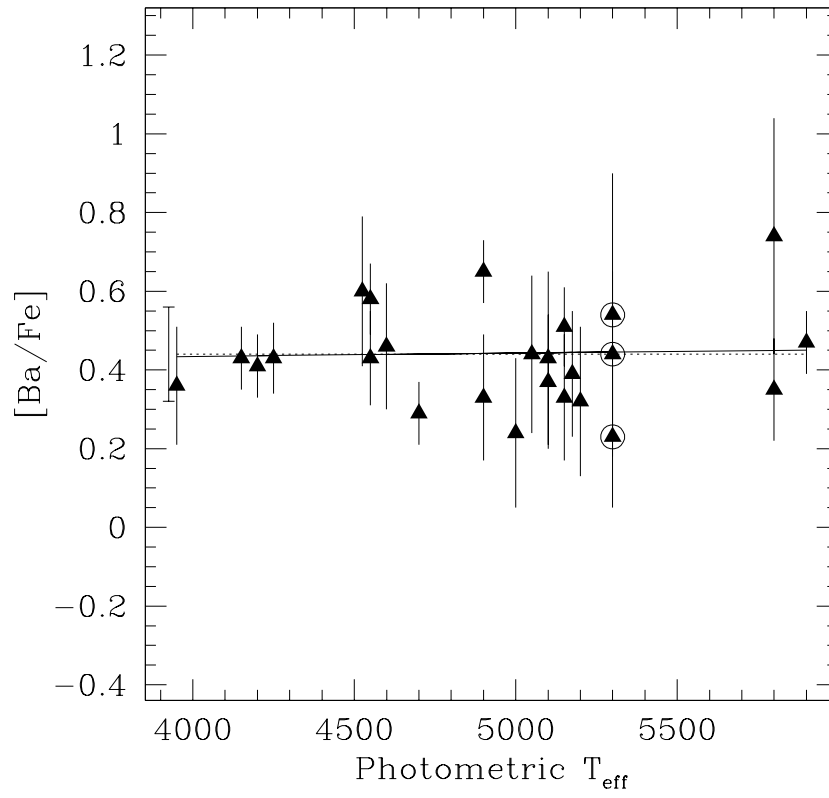


Fig. 22.— $[\text{Ba}/\text{Fe}]$ against T_{eff} . The symbols are the same as in Figure 4.

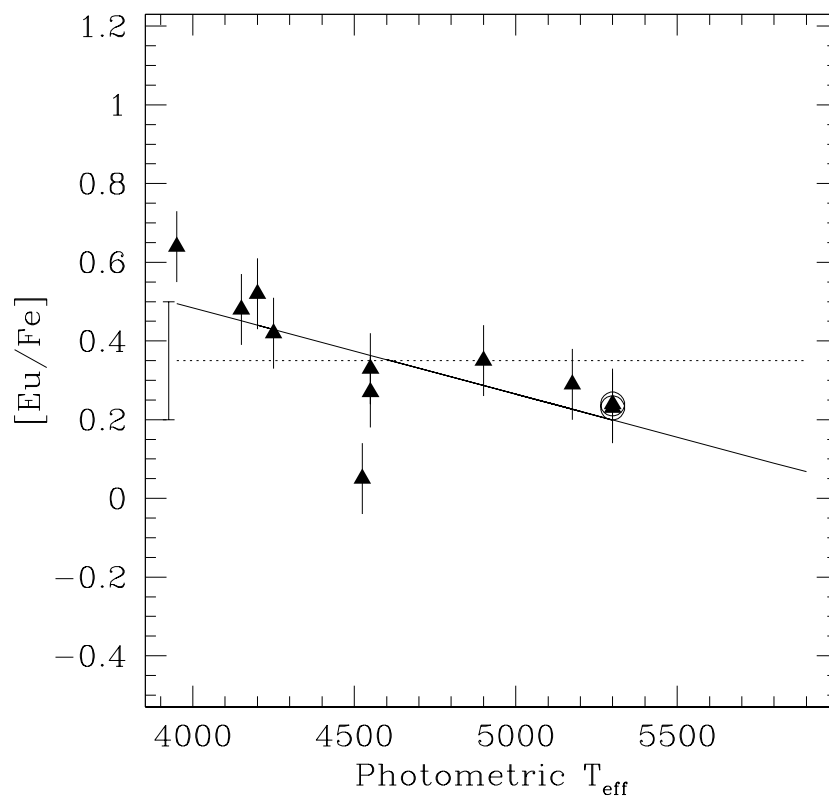


Fig. 23.— $[\text{Eu}/\text{Fe}]$, based on a single Eu II line, against T_{eff} . The symbols are the same as in Figure 4.

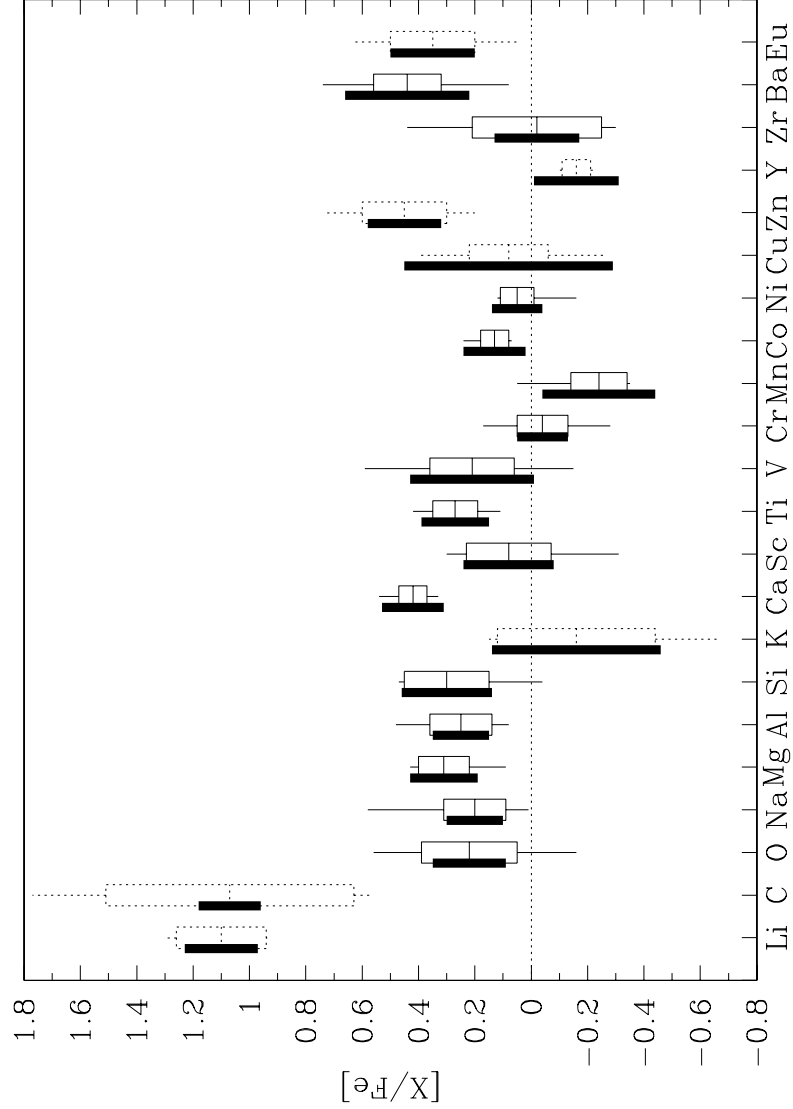


Fig. 24.— Summary of abundance ratios. Each abundance ratio is plotted with a box, which central horizontal line is the mean abundance ratio, the bottom and the top shows its standard deviation, and the vertical lines coming out of the box mark the position of the most deviant points of the sample. The thick line on the left side of the box is the predicted error, which included the dependence on the stellar parameters and the equivalent width determination.

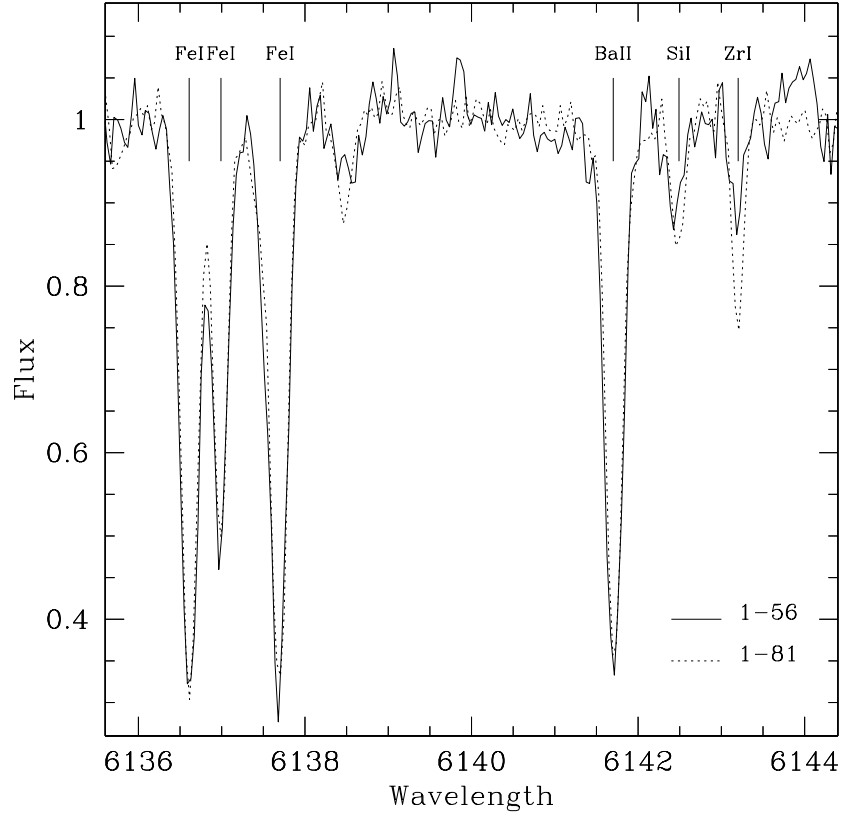


Fig. 25.— Comparison of the strength of the strongest Zr I line included in our study between two stars of similar effective temperatures, 1-56 (4525 K, $[\text{Zr}/\text{Fe}]=-0.44$) and 1-81 (4550 K, $[\text{Zr}/\text{Fe}]=+0.12$). The scatter shown by $[\text{Zr}/\text{Fe}]$ might be due to real abundance variations among stars of different T_{eff} .

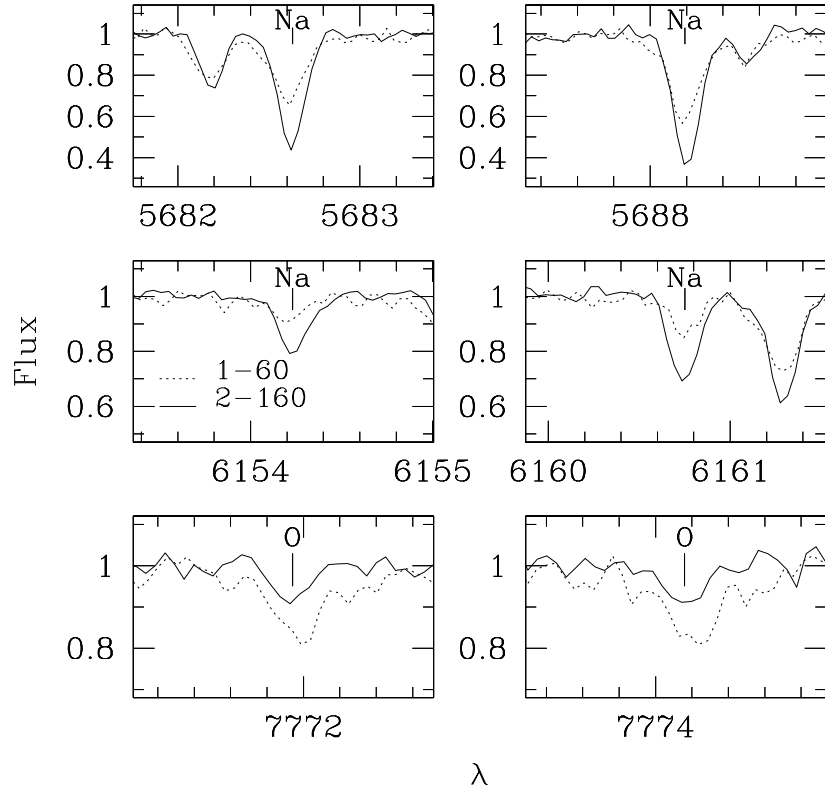


Fig. 26.— Comparison of the strength of four Na I and two O I lines between two stars of similar effective temperatures, 1–60 (4900 K, $[\text{Na}/\text{Fe}] = -0.08$, $[\text{O}/\text{Fe}] = +0.61$) and 2–160 (5100 K, $[\text{Na}/\text{Fe}] = +0.20$, $[\text{O}/\text{Fe}] = -0.11$). The scatter shown by $[\text{Na}/\text{Fe}]$ and $[\text{O}/\text{Fe}]$ is due to real abundance variations among stars of different T_{eff} .

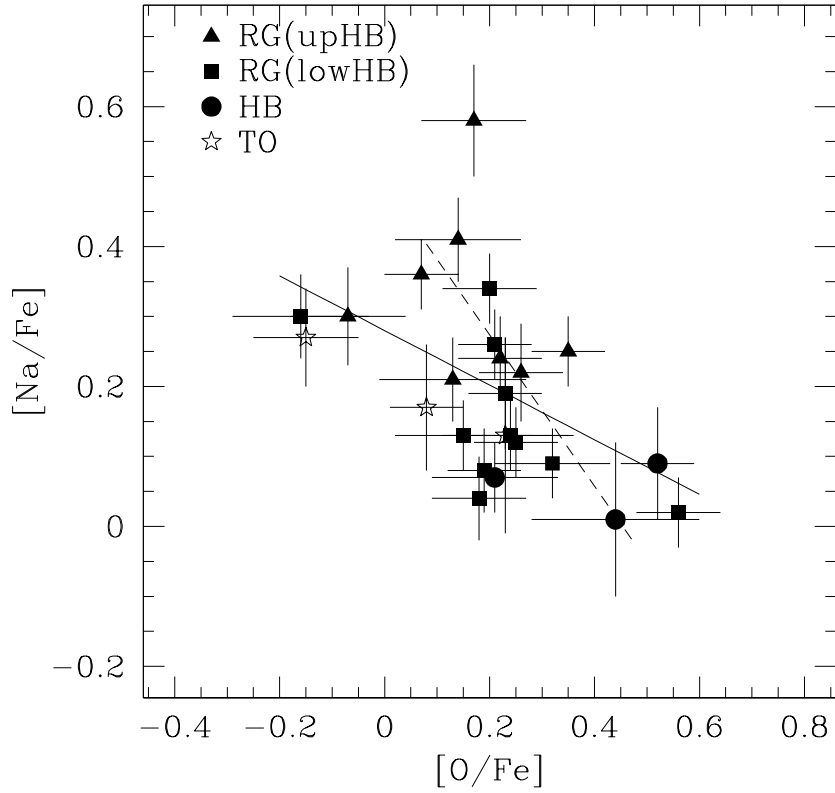


Fig. 27.— $[\text{Na}/\text{Fe}]$ against $[\text{O}/\text{Fe}]$ for M71 stars. Filled triangles are RG stars brighter than the HB, filled squares are RG stars fainter than the HB, filled circles are HB stars and “stars” are stars near the main sequence turn off. The solid line represents the least squares linear fit to our data in M71. The dashed line corresponds to the Na–O anti-correlation present in M4 from the analysis of Ivans *et al.* (1999).

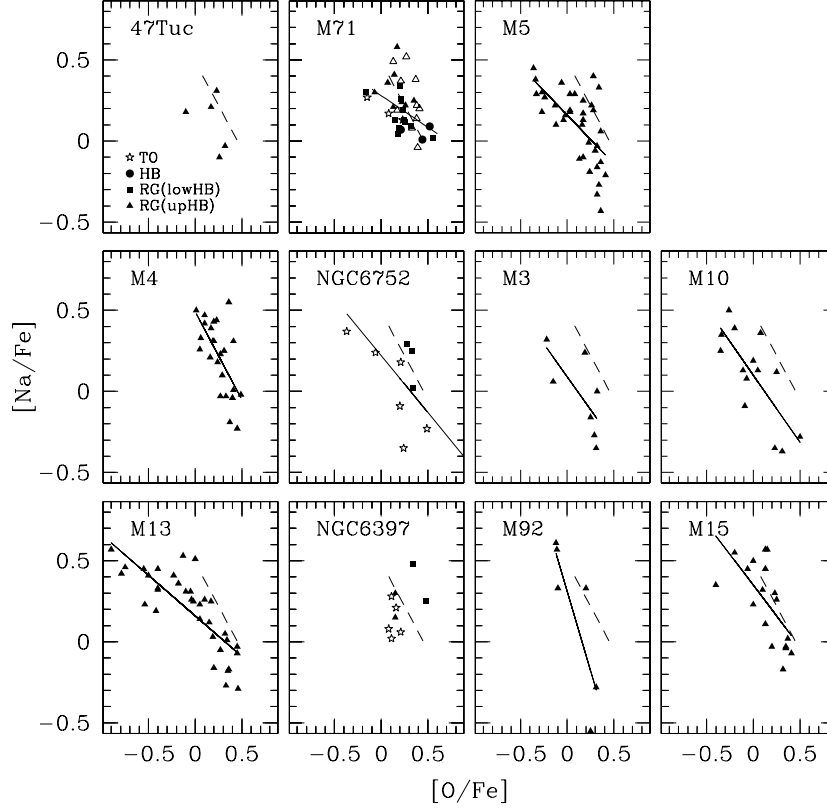


Fig. 28.— $[\text{Na}/\text{Fe}]$ against $[\text{O}/\text{Fe}]$ for M71 and for other globular clusters from the literature. Filled symbols are the same as Figure 27. The literature determinations are: 47 Tuc (Brown *et al.* 1990; Brown & Wallerstein 1992; Norris & DaCosta 1995), M5 (Ivans *et al.* 2001; Shetrone 1996; Sneden *et al.* 1992), M4 (Ivans *et al.* 1999), NGC 6752 (Gratton *et al.* 2001), M3 (Kraft *et al.* 1993), M10 (Kraft *et al.* 1995), M13 (Kraft *et al.* 1993; Shetrone 1996), NGC 6397 (Castilho *et al.* 2000; Gratton *et al.* 2001), M92 (Sneden *et al.* 1992), and M15 (Sneden *et al.* 1997). Open triangles are bright red giants in M71 from the abundance analysis of Sneden *et al.* (1994). The solid lines represent the least squares linear fits of the data from the literature for each cluster. They only shown for those globular clusters where the slope we derive is significant at the 2σ level. The dashed line corresponds to the anti-correlation observed in M4 from Ivans *et al.* (1999), shown as a fiducial line in each panel.

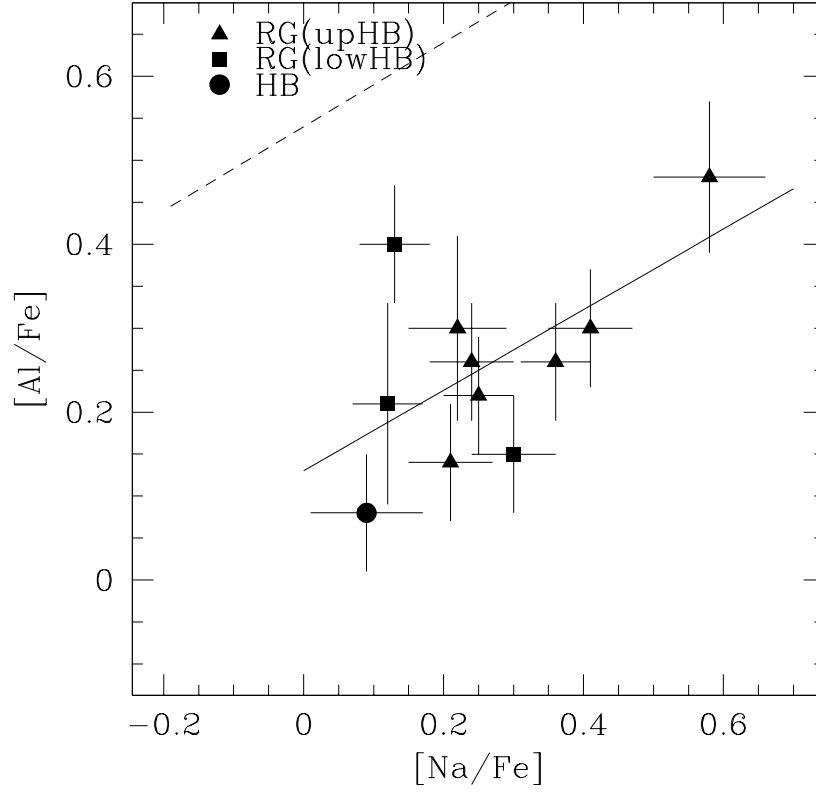


Fig. 29.— $[\text{Na}/\text{Fe}]$ against $[\text{Al}/\text{Fe}]$ for M71 stars. Symbols are the same as Figure 27. The solid line represents the least squares linear fit to our data in M71. The dashed line corresponds to the Na–Al correlation present in M4 from the analysis of Ivans *et al.* (1999).

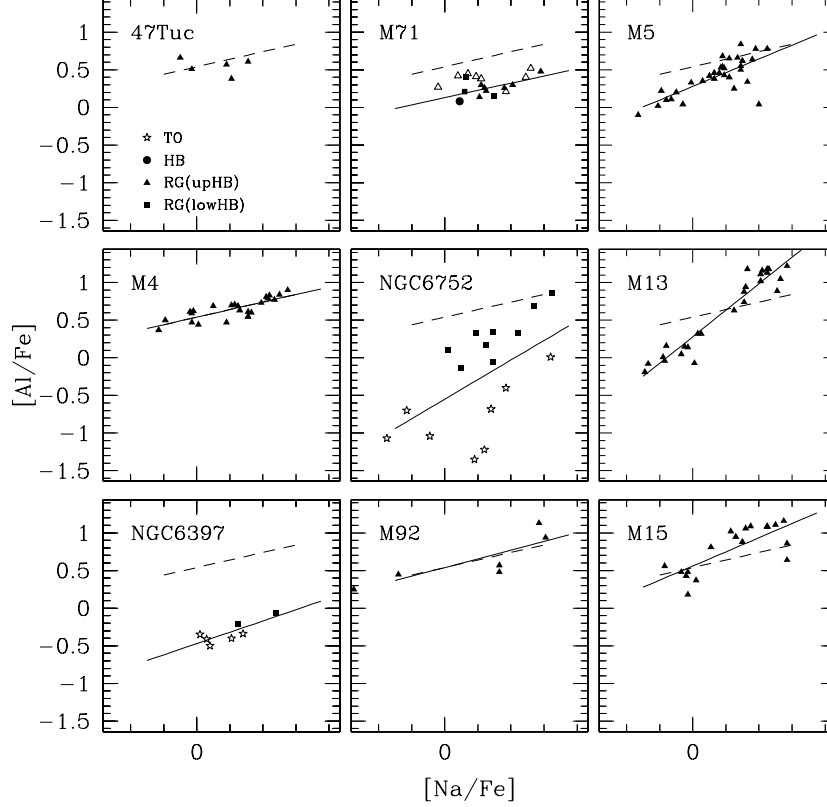


Fig. 30.— $[\text{Na}/\text{Fe}]$ against $[\text{Al}/\text{Fe}]$ for other globular clusters from the literature. Filled symbols are the same as Figure 27. The literature determinations are the same as in Figure 28. The solid lines represent the least squares linear fits of the data from the literature for each cluster. They only shown for those globular clusters where the slope we derive is significant at the 2σ level. The dashed line corresponds to the Na–Al correlation present in M4 from the analysis of Ivans *et al.* (1999), shown as a fiducial line in each panel.

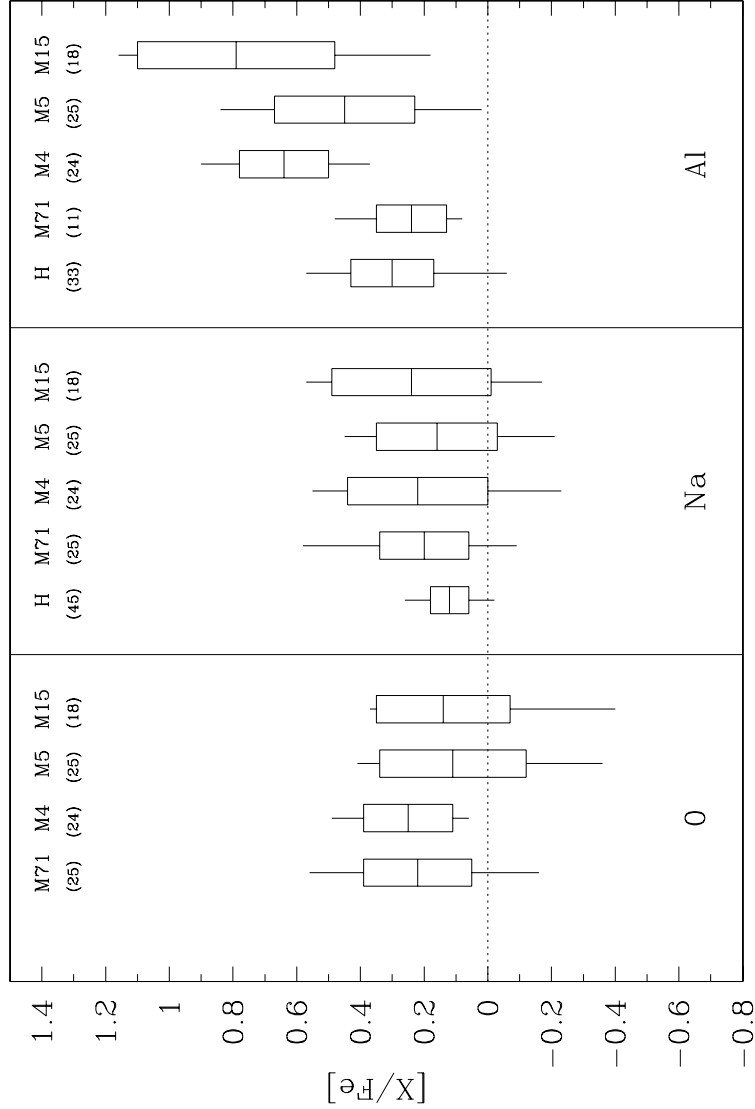


Fig. 31.— Statistical comparison of light elements with mean abundances from halo dwarfs, M4 ($[\text{Fe}/\text{H}] \sim -1.2$), M5 ($[\text{Fe}/\text{H}] \sim -1.2$), and M15 from Fulbright (2000), Ivans *et al.* (1999), Ivans *et al.* (2001), and Sneden *et al.* (1997), respectively. The halo dwarfs plotted in the Figures have been selected from the sample of Fulbright (2000) to have $[\text{Fe}/\text{H}]$ similar to M71 ($-0.6 < [\text{Fe}/\text{H}] < -0.9$). The number in parenthesis indicates the the number of stars analyzed for each element in the corresponding globular cluster. The layout of the statistical box is as in Figure 24.

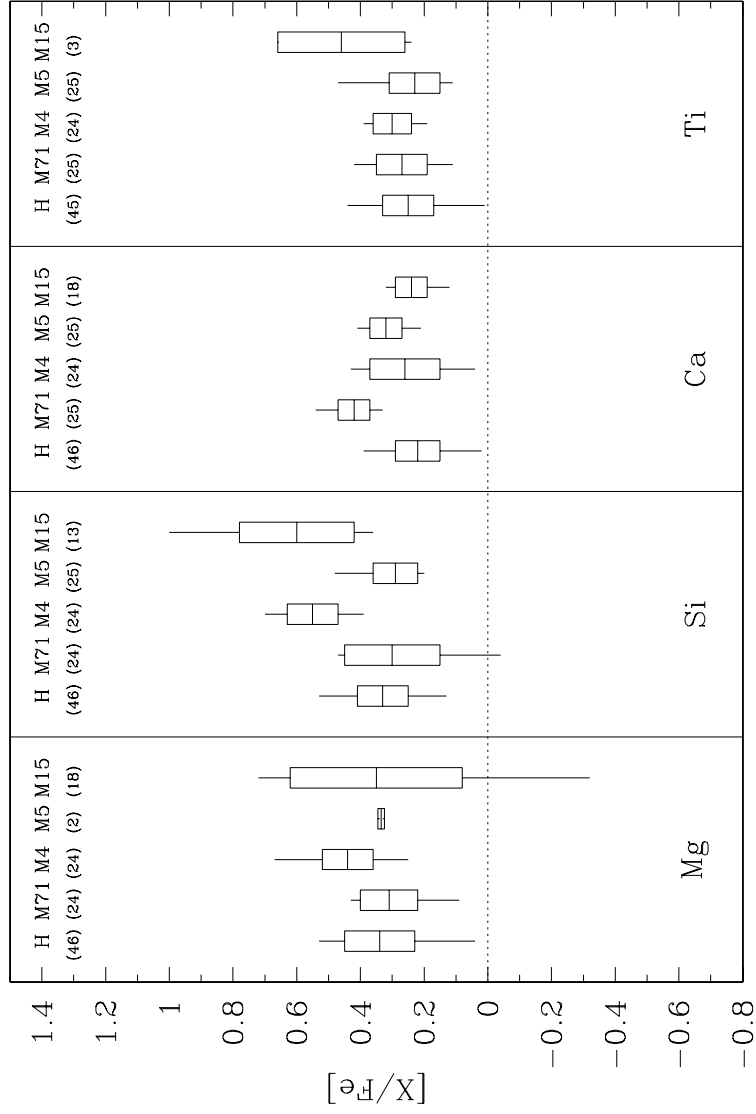


Fig. 32.— Statistical comparison of α -elements. Symbols and references as in Figure 31.

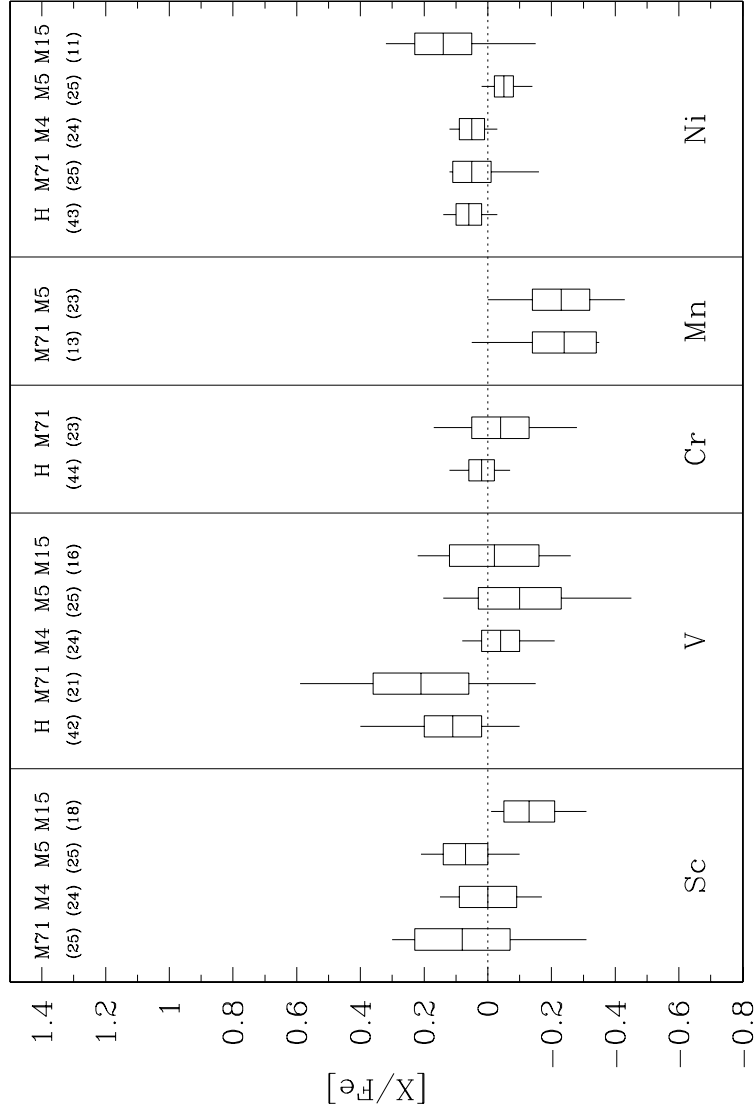


Fig. 33.— Statistical comparison of iron-peak elements. Symbols and references as in Figure 31.

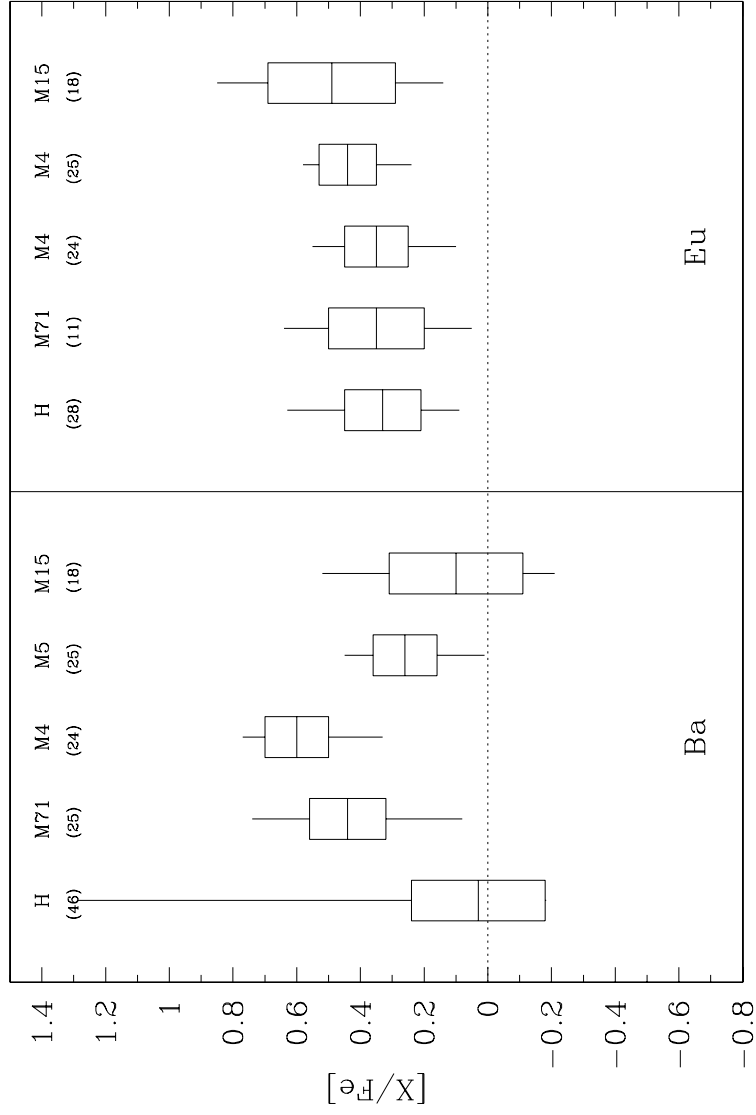


Fig. 34.— Statistical comparison of neutron capture elements. Symbols and references as in Figure 31.